Proposal of a Correlation for Boundary Layer Flow over Real Roughened Surfaces

Università degli Studi di Cagliari

Giorgio Melis

Tutor:
Prof. Natalino Mandas

Dottorato di Ricerca in Progettazione Meccanica
XIX Ciclo

ABSTRACT

Measurements of the flow field around flat plates with different surface roughness are presented. The effects of surface roughness on boundary layer features are analyzed through scaled facsimiles of real turbine blades. Roughness is characterized by small protrusions randomly placed over the surface; moreover, the texture of the blades is defined by parallel grooves created by the manufacturing tool adopted.

The main aim of the present work is to exploit the effect of surface roughness with particular reference to the steam turbine applications.

Four rough plates and a smooth plate were tested at different high Reynolds number conditions and for different incidence angles of the flow respect to the plates.

Roughness characteristics of the plates are typical of the turbine blades, in order to fully understand the aerodynamic efficiency improvement induced by a specific surface texture and to estimate the availability and convenience of manufacturing.

All experimental results regarding the smooth plate are compared with the numerical ones obtained from the 2D cascade code MISES.

Velocity profiles and boundary layer features are presented for all plates.

Skin friction coefficient is estimated and laws of the wall are proposed for different roughness profiles. The effect of the grooves is also investigated.

The experimental data related to surface texture are analyzed and the most representative roughness parameters are underlined; it is found one unique roughness parameter which is representative of the real surface texture.

The law of the wall for rough surfaces is correlated with the roughness parameter proposed.

Moreover, a correlation between technical (sandgrain) and real surface roughness is proposed.

The results presented for the combined effects of roughness and pressure gradients were restricted to the adverse pressure gradient case, due to limitations associated with the measurement campaign. However, the observations seem to corroborate the trends seen at zero pressure gradient.

Acknowledgments

Table of Contents

List of Figures and Tables

Nomenclature

$$C_f = \frac{\tau_w}{\frac{1}{2}\rho U_\infty^2}$$ Skin friction coefficient

$$H = \frac{\delta_1}{\delta_2}$$ Shape factor

k_s Sandgrain roughness height

$$k^+ = \frac{k}{\delta_v}$$ Non-dimensional arbitrary roughness height

PF Peak feed

R_a Average roughness height

R_{tm} Average maximum peak-to-depth height

Re Reynolds number

S_m Mean spacing

$$u_\tau = \sqrt{\frac{\tau_w}{\rho}}$$ Friction velocity

$$y^+ = \frac{y}{\delta_v}$$ Non-dimensional *pitchwise* distance from the wall

$$U^+ = \frac{U}{u_\tau}$$ Non-dimensional flow velocity inside the boundary layer

U_{inf} Freestream (edge) velocity

Greek Symbols

α Incidence angle

β *Staggering* angle

δ Boundary layer thickness (corresponding to $U = 0.99U_{inf}$)

δ_1 Displacement thickness

x

δ_2	Momentum thickness
$\delta_v = \dfrac{v}{u_\tau}$	Viscous sublayer characteristic length
$\kappa = 0.41$	von Karman constant
μ	Dynamic viscosity
$v = \dfrac{\mu}{\rho}$	Kinematic viscosity
ρ	Density
$\tau_w = \mu \left. \dfrac{\mathrm{d}U}{\mathrm{d}y} \right|_{y=0}$	Wall shear stress
Λ_s	Shape/density roughness parameter

I. Introduction

1.1 Background

The overall efficiency of turbines is greatly influenced by blade surface finish. Usually, blade surface is roughened by the specific manufacturing process employed [2, 3], i.e. intrinsic roughness. Surface roughness also increases during lifetime of a turbine (till ten times more than its initial value), due to corrosion, erosion, deposition (ageing) [4]. In the latter case, it is also possible to observe a temporary recovery of efficiency, for instance during a second start-up of the turbine, which blows away the particles and impurities that have been first deposited on the blades.

Figure 1.1 and figure 1.2 show the impact of surface roughness on the losses of each turbine stage for one specific design of turbine. Specifically, stage efficiency is shown on figure 1, while loss in power output is shown on figure 2.

The detrimental effect of surface roughness on steam turbine blades is more pronounced on high and intermediate pressure stages (HP and IP) respect to the low pressure blades (LP stages), owing to the presence of smaller flow areas (i.e. narrow passages for deposits) [13].
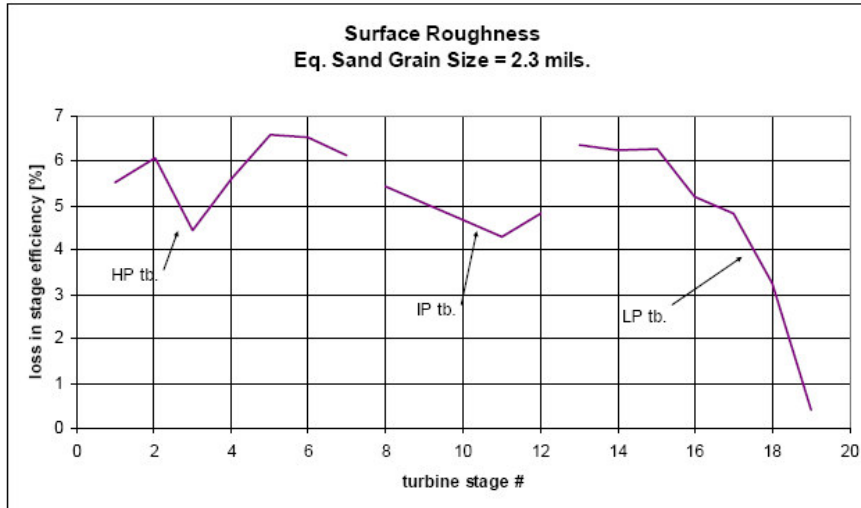
Figure 1.1 Efficiency losses of steam turbine stages due to surface roughness. (courtesy of Encotech Inc.)
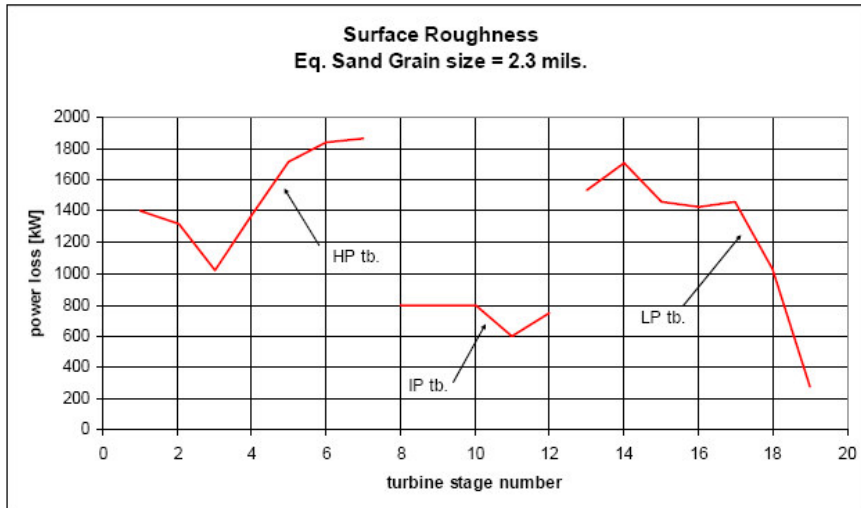
Figure 1.2 Power output losses of steam turbine stages due to surface roughness. (courtesy of Encotech Inc.)

Most of the past experimental works on surface roughness [5] refer to sandgrain roughness, usually obtained by gluing

2

emery paper on the surface. This kind of roughness is generally characterized by equally displaced geometrical roughness elements [6, 7], which are much smaller than the boundary layer thickness [54].

Sandgrain roughness falls into three categories, depending on the roughness height in non-dimensional log-law co-ordinates. In the hydraulically smooth regime, the roughness elements are buried within the viscous sublayer ($k^+ < 5$) and have no effect on the flow.

When roughness elements are so large that they eliminate the entire viscous sublayer ($k^+ > 60$), they fall within the fully rough flow region, which is independent of viscosity. In between these two extremes is the transitional regime ($5 < k^+ < 60$), in which the roughness begins to affect the flow by reducing the sublayer thickness [55].

Surface roughness generally does not affect laminar flows (apart from causing the transition to turbulence), but it can significantly influence the turbulent boundary layer by disturbing the viscous sublayer [56]. Laminar flow is characterized by ordered flow motion, since fluid particles tend to stay aligned in layers with only molecular momentum exchange occurring between layers. In contrast, there is considerable mixing motion between fluid particles within a turbulent boundary layer, which has only a very thin viscous sublayer. Roughness elements larger than the viscous sublayer can therefore easily damage the boundary layer in turbulent flow.

There has been some prior research concerning the general effects of roughness on a boundary layer. It is well-known that roughness increases the boundary layer thickness compared to that of a smooth wall [54]. Roughness also causes a velocity defect in the inner region of the flow near the wall [56]. This is best illustrated by a plot of velocity profiles for rough surface in logarithmic co-ordinates (figure 1.3). Increasing the roughness height displaces the velocity profile downward. The effect of roughness can be viewed as a change in the velocity jump

across the viscous sublayer, which is effectively the same as shifting the origin of the smooth wall profile. Additionally, other research has shown that surface imperfections with a height greater than the viscous sublayer increase the skin friction on a flat plate [9]. While sandgrain roughness significantly affects the inner region of the boundary layer, research indicates that the outer region remains undisturbed by the roughness elements [56].
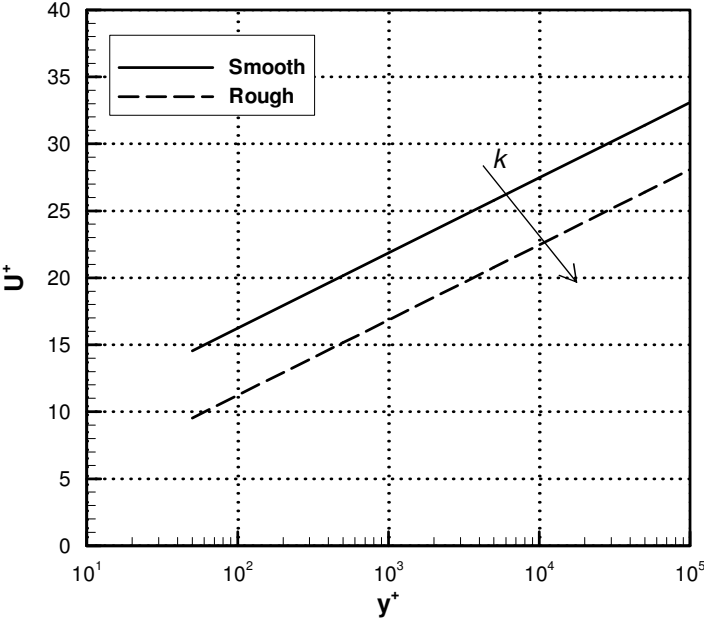
Figure 1.3 Non-dimensional velocity profiles for smooth and rough surfaces. *k* is an arbitrary roughness height

In general, roughness seems to lengthen the interaction and decrease the fullness of boundary layer profile.

A fuller profile can withstand a higher pressure gradient and is therefore less likely to separate due to its higher level of mean kinetic energy.

Antonia and Luxton [48] studied the effect of a step change from a smooth to rough surface for an incompressible turbulent boundary layer. Their results reveal that near the step change,

4

the structure of the internal boundary layer is independent of the undisturbed outer layer. The flow near the wall readjusts rapidly to the new surface condition, and a length of less than twenty boundary layer thicknesses is required for the mean flow parameters, including the shape factor, to attain values identical to those of an entirely rough surface.

Very few experimental studies have inspected roughness effects on the boundary layer of turbine blades, by testing roughened models at low Reynolds number [14]. Moreover, surface roughness effects were estimated after measuring the total pressure losses downstream of a turbine airfoil [32] or in the wake of a turbine cascade [42, 49]. These experimental works refer to high roughness values (typical of the gas turbine blades) and to relatively low Reynolds number.

It has to be underlined the importance of deeply investigate the boundary layer over real roughened surfaces, in the flow condition typical of an on duty turbine.

To understand the effect of surface roughness it is necessary to deeply investigate the boundary layer and analyze the mean velocity profiles. The measured rough wall velocity profiles are not as full as smooth wall profiles [45], as a result of the momentum loss caused by viscous and turbulent dissipation from wakes and shocklets produced by the individual roughness elements.

A significant amount of research has been done on surface roughness, with the majority of it focusing on sandgrain roughness. But often times, the multifarious surfaces of a turbine blade cannot be successfully quantified by a single parameter, such as an equivalent sandgrain roughness. This, in turn, leaves the prospect of developing a correlation that does not involve the use of equivalent sandgrain roughness [3].

Texture of real surfaces is far from being either uniform or isotropic, since it has fully three-dimensional profile. Therefore, blade surface cannot be well described by only on of the commonly used statistical quantifications of surface roughness, such as R_a, but it is necessary to consider many roughness

entities. On the other hand, in the aim of find a universal law for the velocity profile inside the boundary layer flow, it is necessary to summarize all real roughness features within a unique parameter.

1.2 Motivation for this Survey

The main aim of the present research is to derive the law of the wall for rough surfaces, which means find a correlation between surface roughness parameter and main boundary layer features.

The research is oriented to find an innovative tool to be applied when designing of turbine blades, in order to predict the boundary layer losses. Moreover, the achieved model gives quantitative indication of roughness parameters which can be used during manufacturing.

It is important to understand how surface roughness influences the flow inside the boundary layer, and how losses are generated. What is achieved is a *universal* model that has to be applied to a variety of flow condition (i.e. a wide range of Reynolds numbers) and surface textures. Therefore, the experimental data refer to different value of Reynolds number, pressure gradient, roughness parameters and orientation of the protrusions.

The model is developed for predicting boundary layer losses of turbine blades, but the general form and the wide range of data on which is based allow to apply the achieved correlation to many cases that fall in the range of flow conditions analyzed.

A lot of effort is devoted to find one roughness parameter which is representative of real surface texture and is defined from measured roughness values. Therefore, the model is even more general since it is based on this unique surface roughness parameter, which is following correlated with sandgrain roughness.

Moreover, the experimental results are obtained from surfaces that are not the usual approximated roughness, but instead a scaled facsimile of actual turbine blade surfaces.

In this way, the correlations that emerge from the present research are even more endorsed.

1.3 Thesis Overview

This thesis is organized in a manner that will first provide the reader with an insight of the topics at hand, then explain the methodology, and end in an analysis of the experimental results.

The main idea of the author when developing the present work is to put in evidence the results and their field of applicability. Therefore, it is presented only a brief overview of the basic concepts, for the details of which the author suggests more complete texts. Moreover, an effort was devoted to reduce the number of equations, trying to put only the strictly necessary ones.

This is the case of Chapter II where it is given a general insight concerning the boundary layer flow. All main features are analyzed with an emphasis on surface roughness influence.

The same philosophy was adopted for Chapter III, which describes all main tools adopted for the analysis of a surface texture. Furthermore, there is an overview of some real roughened surfaces like turbine blade ones and of the parameters used for describing these surfaces. The analytical expressions of the main surface roughness parameters are quoted on Appendix A.

Chapter IV shows all details regarding the experimental facilities and the measurement instruments, i.e. the wind tunnel and the profilometer apparatus. The measurement protocols are quoted as well.

All procedures adopted when analyzing the achieved data are described on Chapter V. A description of how the boundary

layer experimental data were processed in order to achieve all main boundary layer features is provided. It is also included the depiction of the numerical data used as an important reference for the analysis of some experimental results concerning smooth surfaces.

Moreover, Chapter V discusses the procedure adopted for exploiting the shape/density parameter and how the equivalent sandgrain roughness can be following deduced.

Chapter VI explains all results through many charts. Main boundary layer parameters are shown for all cases analyzed. Comparison between all plates allows to quantify the influence of roughness. Correlations between non-dimensional velocity profiles (i.e. law of the wall) and main roughness parameters are also presented.

Conclusions are marked on Chapter VII together with important recommendations for future works.

II. Boundary Layer Theory

2.1 Introduction

In the present chapter the basic concepts on boundary layer theory are presented with particular emphasis on those features that are investigated in the current research. For a complete exploiting of the boundary layer theory the reader can refer to specific works (e.g. [54, 56]).

2.2 Basic Concepts

The boundary layer is the thin region of thickness δ near the wall in which the flow velocity U decreases from the freestream value U_{inf} at the boundary layer edge to zero at the wall, where the no-slip condition must be fulfilled. Viscosity cannot be neglected in the boundary layer.

The boundary layer thickness δ is defined as having a y value (vertical distance from the wall) for which the velocity U is equal to 99% of the freestream velocity U_{inf}.

There are two types of boundary layers, laminar and turbulent, and for a smooth plate with zero pressure gradient Reynolds numbers having values greater than 1×10^6, generally indicate fully turbulent flow for external flow.

As shown in Figure 2.1, the boundary layer velocity profile merges smoothly and asymptotically into the freestream, making δ difficult to measure.
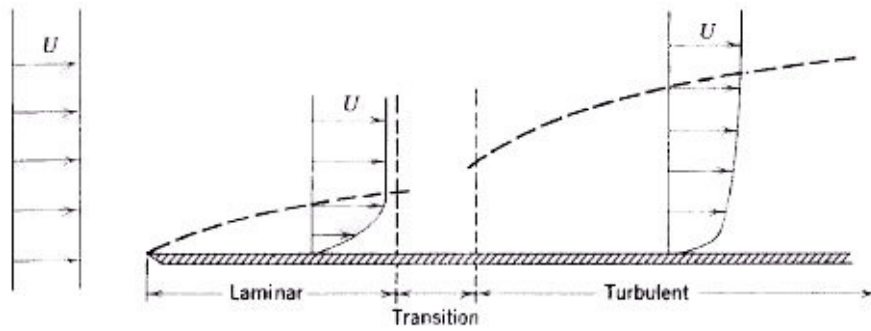
Figure 2.1 Boundary layer on a flat plate (vertical thickness exaggerated for clarity) [56].

Many features are influencing the boundary layer flow other than the aforementioned Reynolds number, that are surface roughness, turbulence levels, and pressure gradients and they can also affect transition to turbulent flow.

An equilibrium boundary layer is defined as one which is in equilibrium with the local shear stress at the wall, and therefore exhibits some degree of self-preservation when described by local length and velocity scales. In contrast, a non-equilibrium boundary layer is changing relatively rapidly with streamwise location, and therefore some or all of the boundary layer cannot be described by local conditions alone. Non-equilibrium boundary layers generally exhibit some dependence on upstream conditions, as well as dependence on additional length and/or velocity scales.

For the purpose of finding self-similar profiles, the boundary layer must be divided into the inner and outer layers (Townsend 1956). In the inner layer, the flow is presumed to depend only on the wall shear, the fluid properties, and the distance from the wall. Under these conditions, a dimensional analysis of the boundary layer flow was performed [54] and this carried to the following momentum equilibrium equation, which is called von Karman integral equation:

10

$$\frac{C_f}{2} = \frac{d\delta_2}{dx} + (2 + H)\frac{\delta_2}{U_\infty}\frac{dU_\infty}{dx}$$

The equation describes the turbulent (steady and incompressible) boundary layer flow over smooth plate, with x representing the direction of the flow.

The equation relates the most important boundary layer integral parameters that are following described.

2.2.1 Displacement Thickness

Streamlines outside of the boundary layer are deflected by an amount called the displacement thickness.

$$\delta_1 = \int_0^\delta \left(1 - \frac{U}{U_{inf}}\right)dy$$

An increase in displacement thickness can lead to some detrimental effects, since it amplifies the viscous effects felt by the outer inviscid flow field.

2.2.2 Momentum Thickness

The momentum thickness is a measure of drag [54].

$$\delta_2 = \int_0^\delta \frac{U}{U_{inf}}\left(1 - \frac{U}{U_{inf}}\right)dy$$

An increase in momentum thickness causes more entropy production through the viscous forces in the boundary layer, which leads to increased profile drag.

2.2.3 Shape factor

The incompressible shape factor characterizes the fullness of a boundary layer profile and is the ratio between displacement thickness and momentum thickness.

$$H = \frac{\delta_1}{\delta_2}$$

A full boundary layer profile has a higher energy level and is less susceptible to separation than a profile that is less full. The

higher the shape factor is, the less full is the velocity distribution within the boundary layer.

The shape factor is heavily dependent on the external pressure gradient, and separated boundary layers show $H \sim 3 \ldots 4$.

2.2.4 Skin Friction Coefficient

Skin friction is a parameter that characterizes the near-wall flow behavior. The local skin friction coefficient is the ratio between the shear stress at the wall and the kinetic pressure of the freestream flow:

$$C_f' = \frac{\tau_w}{\frac{1}{2}\rho U_\infty^2}$$

Where the wall shear stress is proportional to the velocity gradient at the wall:

$$\tau_w = \mu \frac{dU}{dy}\bigg|_{y=0}$$

A full boundary layer profile has a large velocity gradient dU/dy near the wall and therefore more skin friction compared to a less full profile.

All the equations written above show that the complete knowledge of the velocity profile inside the boundary layer, allow to estimate the integral parameters.

2.2.5 Law of the Wall

In the attempt of finding a universal velocity profile law which is valid inside the boundary layer, the vertical distance and the velocity are written in the following non-dimensional form:

$$y^+ = \frac{u_\tau y}{\nu}$$

$$U^+ = \frac{U}{u_\tau}$$

the friction velocity u_τ is defined from the wall shear stress:

$$u_\tau = \sqrt{\frac{\tau_w}{\rho}}$$

while δ_v is a representative length of the viscous sublayer:

$$\delta_v = \frac{v}{u_\tau}$$

$$y^+ = \frac{y}{\delta_v} = \frac{u_\tau y}{v}$$

it is now possible to define the law of the wall:

$$U^+ = \frac{1}{\kappa}\ln y^+ + B$$

The universal logarithmic profile describes the mean streamwise velocity in the overlap region between the inner and outer layers of any wall-bounded flow and is the best known result of the stated classical idea. The log-law has been derived independently by some authors (see Prandtl, von Karman, Millikan). Among various laws that have been proposed recently in addition to the log-law, the power law [52] produces the best fitting of data. Both log and power laws approximate in a similar way the experimental data, since power law better fits experimental data in the inner region (near the wall), while log-law reveals to be efficient approaching the outer layer. A drawback of the power law is that it does not apply at the outer edge of the boundary layer, where a wake function is necessary to complete the inner power law. The everlasting debate is still open, but not only *historical* reason convinced the author of the present research to accept and adopt the log-law.

The *B* constant is accepted to be fairly independent from the Reynolds number [29], and the κ constant is known as the von Karman constant. The two constants of the law of the wall assume the following values for a zero-pressure gradient turbulent boundary layer flow over a smooth surface:

$$\kappa = 0.41$$
$$B = 5.5$$

The values of $y^+ = 5$ denotes the upper limiting value for the laminar layer, which is the region attached to the wall inside the boundary layer. In this zone viscous effects are predominant, since turbulence production is balanced by viscous dissipation and, inside this layer, turbulence cannot sustain itself. For $y^+ > 30$ there is the inertial sublayer, where the log-law is valid, while between laminar and inertial layers there is a not-well bordered region (buffer layer) ruled by a linear law of the wall ($U^+ = y^+$).

2.2.6 Coles' wall-wake Profile

Coles suggested that the standard zero-pressure gradient profile of a turbulent boundary layer with a linear and a logarithmic sublayer could be modified through the addition of a wake function that comes into effect gradually as the outer edge of the boundary layer is approached:

$$U^+ = \frac{1}{\kappa}\ln y^+ + B + \frac{\Pi(x)}{\kappa}w\left(\frac{y}{\delta}\right)$$

The wake function $w(y/\delta)$ describes how the wake modification comes into effect with increasing y:

$$w\left(\frac{y}{\delta}\right) = 2\sin^2\frac{\pi \cdot y}{2\delta}$$

Π may vary with x and describes how retarded the boundary layer is and how well-developed the wake region is. Coles gives:

$$\Pi(x) = \kappa\frac{\delta_1 U_\infty}{u_\tau\delta} - 1$$

2.3 Pressure Gradient Effects

When a pressure gradient is introduced, the streamwise velocity varies with respect to x. For a favourable pressure gradient, freestream velocity increases along the streamwise direction and in turn causes the boundary layer to develop

more rapidly. The opposite holds true for an adverse pressure gradient.

A variety of methods have been developed to investigate the effects of pressure gradients on turbulent boundary layers. One such method is an extension of the previously noted von Karman integral relation. Like before, this integral method is one in which ordinary differential equations are averaged across the boundary layer (White).

Assuming $U_{inf}(x)$ is known, the equation is left with the three unknowns δ_2, H, and C_f. On reference [56] the details of this analysis are quoted.

2.4 Roughness Effects

As additional surface roughness is introduced to a system, the structure of the boundary layer near the wall is altered causing an increase in skin friction drag.

Flow structure over a rough surface is dominated by the wakes created by the roughness elements. In general, the flow in the roughness sublayer is markedly different from that in the viscous sublayer of a smooth surface, and become spatially non-homogeneous just above the roughness elements.

From many experimental investigation of the flow inside the boundary layer (even since 1971 [48]), it is apparent that the turbulent transport mechanisms near the wall depend strongly on the surface geometry and it is reasonable to conjecture that any turbulence model which does not explicitly take into account the surface geometry will not be able to properly predict the transport characteristics of the flow.

The similarity hypothesis of Townsend (1976), states that the turbulent flow in the region outside the roughness sublayer is independent of the wall roughness at sufficiently high Reynolds numbers. Inside the boundary layer it is possible recognize two regions, the one attached to the wall (the internal boundary layer) whose properties are dominated by the turbulence generation over the rough surface and by the wake of the first

roughness element, and the external boundary layer, where the flow has the same characteristic as the original smooth wall boundary layer.

Presuming the surface has a uniform average roughness height k, this can be compared with the viscous length δ_v, and it is possible to identify three different flow regimes. When k^+ (k/δ_v) is lower than 5 the surface is defined hydraulically smooth, i.e. the surface asperities fall inside the viscous sublayer and do not manifest their influence on the flow. The range of k^+ between 5 and 60 defines the transitional-roughness regime, while a fully rough flow is characterized by $k^+ > 60$.

2.5 Riblets

The presence of grooves over the surface can alter the flow structure of the boundary layer [11]. These structures called riblets are characterized by an alternation of peaks and valleys which induce a regular change in flow shear stress. The generated streamwise vortices alter the momentum exchange properties inside the boundary layer.

Currently, the mechanism for the riblet's ability to reduce viscous losses is not fully understood [39]. It is proved that riblets reduce the momentum exchange near the surface, besides enhancing the possibility of boundary layer separation.

Computational Fluid Dynamics (CFD) has been decisive in exploring curiosities related to riblets and more generally to near wall turbulence. It has been observed the interaction between the riblets and the time-dependent motion of near wall turbulence structures, such as persistently rotating clumps of fluid or vortices. Calculations show that riblet grooves effectively maintain a thin, non-turbulent layer in the near-wall region, protecting the wall from inrushes of turbulent, high momentum, drag producing fluid.

2.6 Numerical Analysis

Modern predictive methods for calculating boundary layers at applicable Reynolds numbers must use turbulence models, since direct numerical simulation (DNS) of the Navier-Stokes equations is well beyond the reach of present day computers except for very low Reynolds numbers. Model developers must then rely on the experimental data base to formulate and validate new models. Unfortunately, because of the expense of large scale facilities, and the difficulty in accurately measuring high Reynolds number flows, the vast majority of the available data have been acquired at low Reynolds numbers.

Roughness is numerically simulated by changing the mixing length of the turbulence model near the wall, but only a detailed modeling of the roughness structures can lead to appreciable results. Therefore, it is of relevant importance to find the law of the wall for rough surfaces to be following implemented on a numerical code. The achieved law of the wall must rely on a roughness parameter which is able to describes the overall texture of the real surface.

III. Surface Roughness Statistics

3.1 Texture Parameters

Surface roughness can be described using many parameters that are statistically evaluated after a measurement of the texture characteristics. One of the most important surface parameters is the average roughness R_a, which gives a good general description of the height variations in the surface. The following figure shows a cross section through the surface, where a mean line is first found that is parallel to the general surface direction and divides the surface in such a way that the sum of the areas formed above the line is equal to the sum of the areas formed below the line. The surface roughness R_a is now given by the sum of the absolute values of all the areas above and below the mean line divided by the sampling length. Therefore, the surface roughness value is given by:

Ra=(|area abc|+|area cde|)/*f*.

where *f* is the feed.
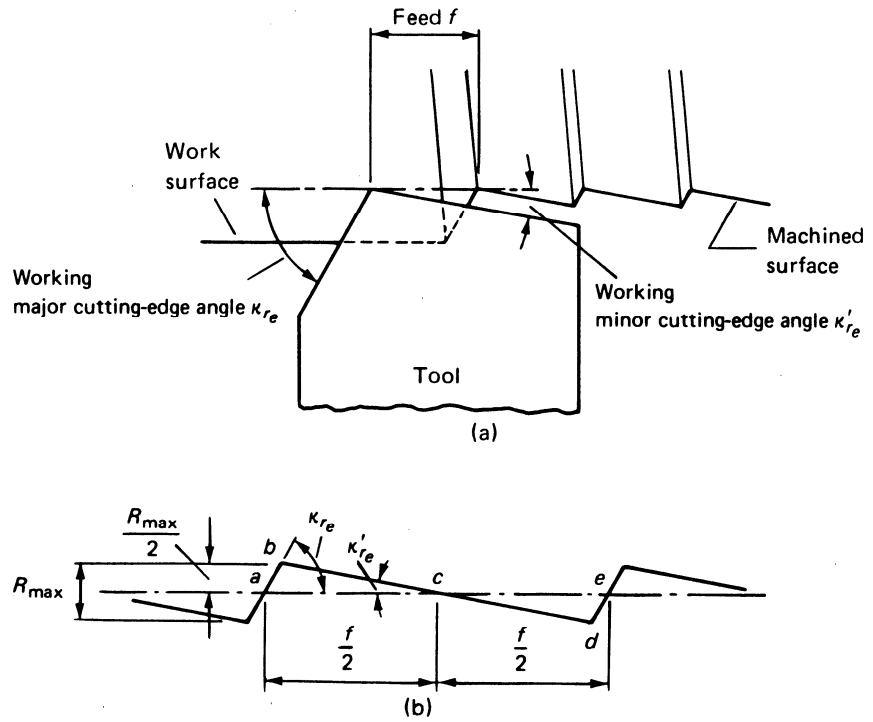
Figure 3.1 Texture of a manufactured surface.

Average centerline roughness R_a is typically used to describe machined surfaces.

Unfortunately, this parameter does not give information on both shape and spacing of the roughness profile. Surface manufacturing on blades, for instance, produces a well-structured roughness, fairly anisotropic; therefore R_a cannot be really representative of all surface texture. For example, R_a does not give any information if the surface is sharp peaks or deep valleys based.

Other parameters can be defined on statistical basis, like the root-mean-square roughness R_q, typically used to describe the finish of optical surface, and the so called wavelengths factors [6].

Many other roughness parameters can be estimated through a deep investigation of the surface, as the ones evaluated during the measurements described in the following Chapter and whose definitions are reported on Appendix A.

For a real rough surface the statistical skewness R_{sk} provides a quantitative measure of the relative concentration and size of peaks and valleys. A positive skewness value denotes the presence of protrusions above the mean line and is typical of surfaces with deposits and erosion. A large negative skewness denotes recess or cavities typical of pitting or spallation [14]. Therefore, skewness is characterizing the degree of asymmetry of a surface about its mean centerline.

Kurtosis R_{ku} is defined as the relative peakedness or flatness of a distribution compared with its normal distribution. A large kurtosis is representative of peaked distributions while a small kurtosis indicates a relatively flat distribution.

3.2 Blade Roughness

As already noted [4, 5], due to the non-uniformity of the blade surface, the commonly used statistical quantifications of surface roughness, such as R_a, are not sufficient. Therefore, the calculation procedures used for rough wall boundary layers of turbine blades must rely on a knowledge of equivalent sandgrain roughness, k_s.

The last one may or may not be similar to any of the measured values and at the present there is no universal expression that relates the various surface characterization values. Many relations between k_s and some measured value have been proposed [1, 3, 16], and the Sigal and Danberg parameter [57] reveals to be the most efficient, since many roughness features are summarized within a unique numerical entity.

Furthermore, the correlations that have been proposed in the past between equivalent sandgrain roughness and the most commonly used roughness parameters were derived for specific cases and applications (e.g. Bammert & Sandstede, Koch & Smith), therefore, with strong limitations in the range of applicability, especially regarding the Reynolds number. Historically, these correlations were based on R_a and R_t, the

former since it is by far the most commonly used industry standard and R_t because it gives a measure of the maximum amplitude of observed surface variations to which the turbine flowfield may be exposed.

Correlations were proposed between k_s and other typical roughness parameters, such as slope angle, skewness and kurtosis [14] or a proper combination of them [Musker].

The lack of universality of the correlations proposed since now is mainly owed to the use of only one measured roughness entity, which cannot be representative of the non-uniformity of the blade surface. Therefore, in the present the aim is to define a unique roughness parameter which incorporates different roughness entities.

3.2.1 Shape/Density Parameter

All rough surfaces analyzed during the present research are characterized by two main roughness scales, therefore two or more different type of parameters have to be taken in consideration to describe roughness effects completely. Furthermore, it becomes crucial to find a unique parameter which summarizes the many roughness entities and the influence of surface anisotropy [5, 10, 41, 43].

The roughness shape/density parameter, Λs was developed by Sigal and Danberg [57] in an attempt to correlate the k_s estimation process to both the spacing and shape of roughness elements. The parameter was originally derived for use with two and three-dimensional roughness elements mounted to a smooth surface. It is defined as:

$$\Lambda_s = \frac{S}{S_f}\left(\frac{A_f}{A_s}\right)^{-1.6}$$

S is the reference area; it is the area of the smooth surface before adding on roughness;

S_f is the total frontal area over the rough surface;

A_f is the frontal area of a single roughness element;

A_s is the windward wetted surface area of a single roughness element.

Since the surfaces being evaluated in this study are real roughened surfaces rather than ordered cones or hemispheres [5, 10], the calculation of A_f, S_f, and A_s had to be adapted accordingly. Therefore, all the above-mentioned entities were defined after assuming a simplified roughness geometry using the available experimental data.

IV. Experiments

4.1 Roughness Measurement Protocol

4.1.1 Plates Manufacturing

Surface texture of the plates was obtained by the typical milling process adopted when turbine blades are manufactured. This process defines two main roughness scales: the first one is showing microscopic irregularities, typical of non-polished surfaces, which are described by many parameters, such as R_a. The larger roughness scale is characterized by visible grooves (see figure 4.1), which are caused by the milling tool employed. Groove spacing is described by peak feed (*PF*), which is the distance between the peaks or valleys of two parallel grooves.

All plates were roughened in a way that the obtained roughness values were geometrically scaled respect to the typical values of a manufactured steam turbine blade. The similitude theory was adopted, specifying same values of both Reynolds number and skin friction coefficient. Therefore, linear correlation allowed predicting exact values of boundary layer parameters (e.g., friction velocity) of the manufactured blades, after measuring the equivalent ones on the tested plates.

On table 4.1 for each plate and for each of the two roughness scales, roughness parameters are quoted.

4.1.2 Surface Roughness Measurement

Plate surface texture was analyzed by an optical profilometer as to achieve a detailed set of surface roughness parameters. The most important of which is the average roughness R_a (or centerline average, *CLA*), but as mentioned earlier, this parameter does not give information on both shape and spacing of the roughness profile. This is why the roughness

measurement protocol was providing the many roughness entities described in the previous chapter and shown on Appendix A.

Profilometer stylus picks up both the surface roughness and the form of the part, therefore an estimation of the grooves was also made and *PF* values were found.
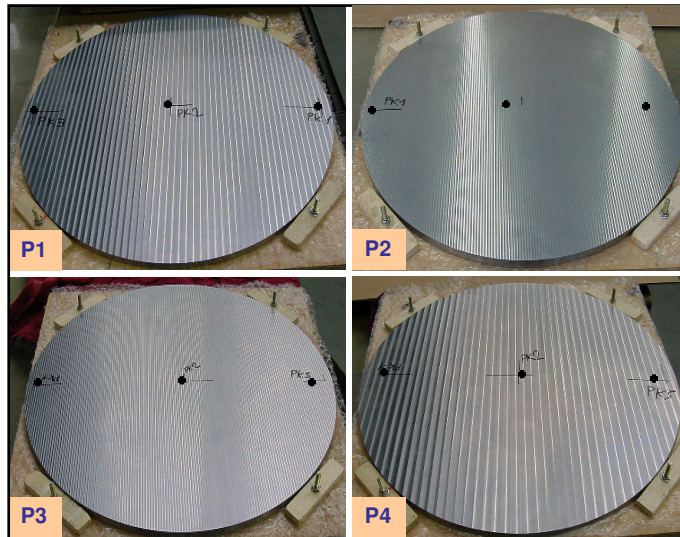
Figure 4.1 Plates' shape and roughness measurement points.

4.2 Boundary Layer Measurements

4.2.1 Plate Test Set of Göttingen

Four "rough" round-shaped plates and a smooth plate were tested at different flow conditions. All tests were executed at DLR, Göttingen and were reported in [17, 23], where all details can be found.

The wind tunnel is a closed-return facility which allowed achieving very high Reynolds number (per unit length, almost till 10^8). Since the wind tunnel is pressurized, the undisturbed velocity is kept almost constant when varying the Reynolds number.

The plates were placed inside the wind tunnel test section (see figure 4.2) by means of a support that allowed them to

rotate around two perpendicular axes. In this way, the rotation around the axis that lies on the plane of the plate, allows the latter to tilt respect to flow direction. Apart from the flat plate condition (i.e. zero-pressure gradient case) it was also tested an incidence angle of 7°, which corresponds to an adverse pressure gradient flow.

Once placed inside the test section apparatus, the plates are allowed to rotate around an axis which is perpendicular to the plate; this rotation allows to change the so called *staggering* angle of the plates, which is the one between the main groove direction and the flow direction. Hence, as stated before, not only the condition where the grooves are aligned with the flow was tested, but also different angles of inclination of the grooves respect to flow direction were analyzed. Different values of the grooves inclination were adopted from plate to plate, apart from the condition of zero-*staggering* angle which was tested for all plates. All values adopted are shown on table 4.1.
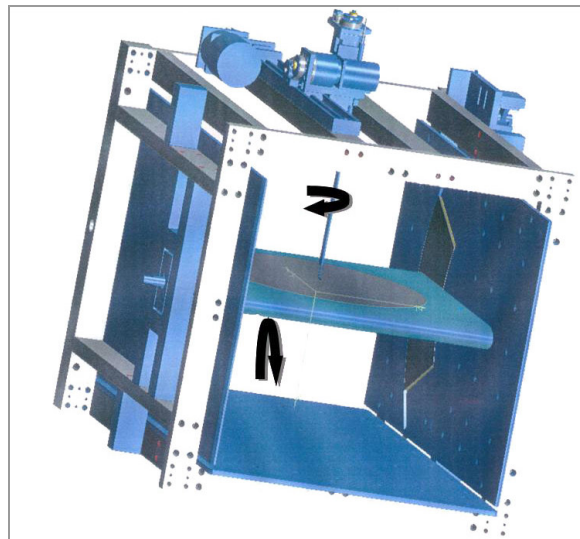
Figure 4.2 Wind tunnel test section.

Three different Reynolds number conditions were tested, whose values are as follows, together with the corresponding

flow inlet velocity. Reynolds numbers are shown per unit length of the plates diameter.

$$Re_1 = 1.54 \ 10^6 \ m^{-1} \qquad \left(U_{inlet}\right)_1 = 25.05 \ m/s$$

$$Re_2 = 7.46 \ 10^6 \ m^{-1} \qquad \left(U_{inlet}\right)_2 = 23.34 \ m/s$$

$$Re_3 = 9.55 \ 10^7 \ m^{-1} \qquad \left(U_{inlet}\right)_3 = 30.14 \ m/s$$

The static pressure was measured after displacing pressure holes over the plates, and the free stream pressure was measured by differential pressure transducer (of piezo-electric type).

The developed boundary layer over the plate was investigated by an aerodynamic probe (Pitot tube), which was moved normal to the plate, along the *pitchwise* direction (in analogy with the blade flow path) and this measurement was repeated at five different axial positions (along flow or *chordwise* direction), as shown in figure 4.3.
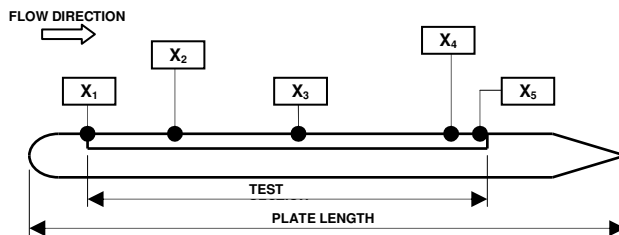
Figure 4.3 Plate geometry and axial locations for BL measurements.

For only some testing configurations, the boundary layer was also inspected by a hot-wire anemometer and the experimental values were compared with those obtained using the Pitot tube. This procedure confirmed the good accuracy of the aerodynamic probe measurements, which was estimated as 3% on kinetic pressure. The hot-wire measurements were made only for the smooth plate and for plate 02 at the two lowest Reynolds number conditions tested (Re_1 and Re_2,

respectively), at zero-incidence angle, and with the grooves aligned to flow direction. During these specific measurements, not only the profile velocity U but also the undisturbed velocity U_{inf} was measured using the hot-wire anemometer.

Some difficulties were found for the Pitot tube measurements made at the leading edge, especially at high Reynolds number, where the boundary layer thickness is low and the probe disturbance is proportionally high.

A resistance strain gage was attached to the wall and was deformed whenever the probe comes in contact with it. In this way, when measuring the Pitot tube is always moved away from the wall (any contact with the latter is avoided) and the boundary layer flow is not significantly altered by the probe.

	PF [mm]	R_a [µm]	*Staggering* Angle β [°]
Plate 01	7.8	4.2	0, 20, 40
Plate 02	3.1	4.2	0, 15, 30
Plate 03	3.1	1.6	0, 15, 30
Plate 04	10.4	4.2	0, 30, 60

Table 4.1 Summary of the plates measuring conditions.

4.2.2 Measurement Uncertainty

There are a few sources of measurement uncertainty specific of the boundary layer pressure data. These uncertainties are mainly caused by the aerodynamic probe measures.

A Pitot tube suitable for boundary layer measurements was chosen, in order to lower the wall proximity error. Furthermore, an accurate calibration of the probe has been performed, taking into account main sources of errors, like the effect of vertical velocity gradient along the probe, the effect of stream turbulence, and the misalignment of the probe with the flow (of about ±1°).

What it is mainly influencing the measurement uncertainty is the vertical positioning of the probe (along y direction), and together with the other source of errors, a global error measurement of 3% on kinetic pressure was estimated.

V. Data Analysis

5.1 Surface Roughness Data

Many roughness parameters were achieved through the measurements made by the optical profilometer as described on Chapter IV. All data are fully analyzed and compared between all plates. Results are shown in the following chapter, where the estimation of the shape/density parameter is also presented.

5.1.1 Shape/Density Parameter

In the case in exam, so called two-dimensional measures over the surface texture were taken, since the contact stylus was moved along two perpendicular directions on three different small zones localized on the entire plate's surface (as described on Chapter IV). Therefore, the surface areas that define the shape/density parameter (see relative expression, Chapter III) were defined from a simplified geometry using the available data, and referring to the following considerations.

S can be defined from the cut-off length (considering a square region surrounding the measurement point), but unfortunately this value changes throughout the measurement protocol without any reasonable relation to the surface texture. The latter is modeled referring to a unique simplified roughness element which lays over a reference region. The surface area S is thus defined from values of mean spacing.

S_f and A_f are considered equal because the following simplification is adopted: all roughness elements are supposed having a tetrahedrical shape.

As it was suggested [10], only half of the A_s value is taken.

5.2 Numerical Simulations

Numerical results obtained from the boundary layer flow simulation of a flat plate are useful not only for comparison with the analogous data carried out from the experiments on smooth surface, but also for capturing important information to be applied to the data reduction process made on the experimental results of the rough plates.

The geometrical model used for the numerical simulation was replying the smooth plate tested in the wind tunnel. The numerical simulation was carried at the same flow conditions, i.e. the three Reynolds numbers and the two incidence angles, that have been tested experimentally.

The 2D cascade numerical code MISES (Youngren and Drela, 1991) [40] was used. It is a finite-volume code based on a viscous-inviscid model that solves the Euler equations coupled with the integral, viscous boundary layer formulation. Many boundary layer entities were computed, such as momentum and displacement thickness, skin friction coefficient and freestream velocity along the flow direction. A typical output from the numerical code is presented in figure 5.1.

The results from MISES code are definitely reliable from a numerical point of view, in fact comparing the values of the main boundary layer parameters that were achieved both experimentally and numerically, they agree very well at every axial position tested. These comparisons are following shown on Chapter VI. It is now worth noting that the numerical simulations are also able to capture some flow features that are visible (see relative charts) from the experimental results, like flow transition to turbulence and pressure gradient effect.
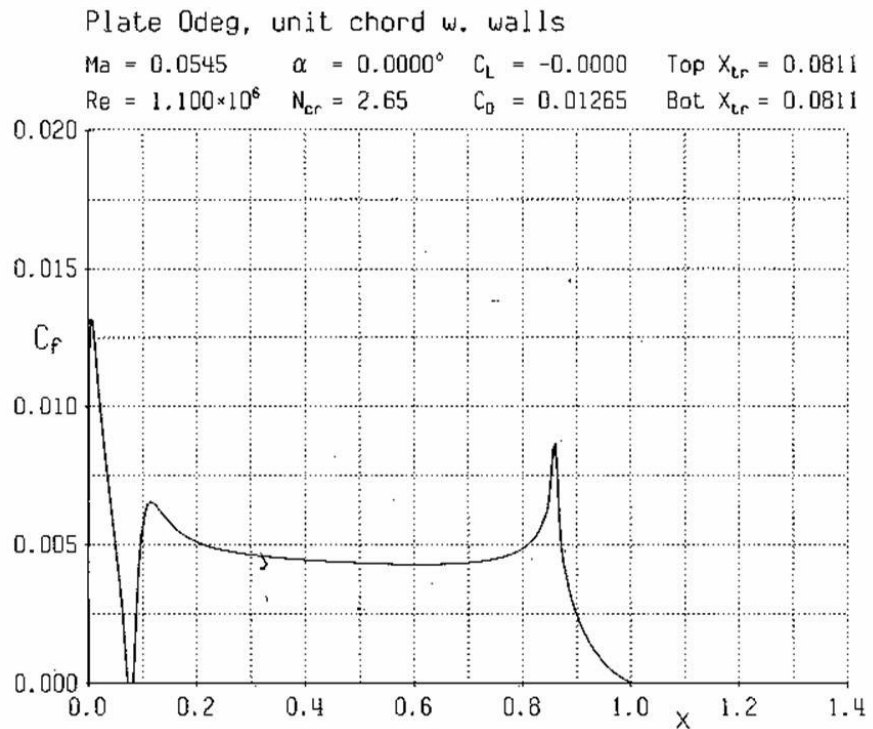
Figure 5.1 MISES output: skin friction coefficient vs. axial direction **x**.

5.3 Boundary Layer Data

The huge amount of data obtained from the wind tunnel experiments is processed in order to fully characterize the flow inside the boundary layer.

The dynamic pressure values given by the Pitot tube allows to compute the velocity inside the boundary layer, which is compared with the undisturbed velocity value. In this way, it is possible to reproduce the velocity profile at the five axial locations tested, for all plates and at all flow conditions analyzed (summarized on Chapter IV).

5.3.1 BL Integral Parameters

The experimental points that define a velocity profile are fitted by a logarithmic function, which is subsequently integrated in order to obtain both displacement and

momentum thickness. The ratio between the last two parameters gives the shape factor (see the equations quoted on Chapter II).

There are several methods for the experimental estimation of skin friction inside a boundary layer flow [7, 27]. As a general approach [19], when studying the flow near the wall, there are mainly three possible choices: the first evaluates the wall shear stress experimentally, through direct methods, such as optical or floating element balance [7], and manometric ones, such as Preston or Pitot tube. Skin friction can also be evaluated from integral momentum method and velocity profile analysis, but this procedure is accomplished by many uncertainties. The third choice is to estimate skin friction relying on the law of the wall.

Another technique for the shear stress (τ_w) measuring is the Clauser's plot method [3]: it requires very detailed velocity measurements, which are achievable only by a high frequency response probe, like a hot-wire anemometer.

Trough accurate tests, as the ones made during the Göttingen experimental campaign, it is possible to achieve reliable values of the velocity inside the boundary layer. The analysis of the velocity profiles allows to estimate the skin friction coefficient. Particularly, it was used the von Karman integral momentum equation (see Chapter II), which requires the knowledge of both the momentum gradient and the freestream velocity gradient, other than the value of the shape factor. It has to be noted that in the proximity of both leading and trailing edges of the plate, high and localized pressure gradients are perceived, and this reflects on the skin friction axial trend.

Once the skin friction value is achieved, wall shear stress and friction velocity are consequently estimated.

5.3.2 Laws of the wall

By using all computations described above, it is possible to estimate the non-dimensional velocity profile (U^+ *vs.* y^+)

according to the equations presented on Chapter II, and also considering the Coles' wake correction function.

This procedure allows to achieve the so called law of the wall for all plates, both smooth and rough ones, at every flow condition tested. As mentioned earlier, and shown in the next chapter, the law of the wall is represented by a straight line in a semi-logarithmic chart, which is obtained from a regression of the experimental data.

Furthermore, roughness should only influence the value of the y-axis intercept of the law of the wall (constant *B*), while the von Karman constant κ remains unchanged. Therefore, in the present work the proposed correlations between roughness entities and boundary layer flow characteristics refer to the following relation, originally proposed by Grigson [43]:

$$\Delta U^+ = U^+_{smooth} - U^+_{rough} = \frac{1}{\kappa}\ln(1+0.3k^+)$$

k is an arbitrary roughness height.

$$k^+ = \frac{k}{\delta_v}$$

The law of the wall has been found strictly valid only inside the inertial (outer) layer, for *y*+ > *30*; therefore, the regression curve adopted when defining the law of the wall, is applied to only those experimental points that satisfy the condition *y*+ > *30*.

5.3.3 Tilted plates

The data analysis procedure described above is applied also to the tilted plate. The main difference relies on the evaluation of the gradients used for computing the skin friction. In general, for the tilted cases, U_{inf} varies along axial position not only because of the plate's tilting but localized gradients are also visible among the leading edge and the trailing edge of the plate. The main aim is to estimate these two effects separately.

As stated before, the skin friction coefficient directly depends on the momentum thickness gradient and on the velocity

profile shape. It could be thought that as the boundary layer becomes thicker, momentum thickness grows up (displacement thickness as well); this is not a general rule, since, for example, when the flow Reynolds number is increased then the velocity profile flatters, both gradients of momentum thickness and velocity decrease and define a lower skin friction value. When there is an adverse pressure gradient, the velocity profile flatters respect to the zero-pressure gradient case at the same axial position, but this tendency is progressively less evident at increasing axial locations. This means that momentum thickness is definitely higher but its axial gradient is lower than the corresponding one at zero-pressure gradient, and this causes the skin friction coefficient to be slightly lower.

When estimating the skin friction coefficient using the von Karman integral momentum equation, it was noted that the contribution given by the momentum thickness gradient is always higher than the one due to the freestream velocity gradient.

A similar reasoning can be applied when comparing the law of the wall between the tilted case and the zero-pressure gradient case. In fact, for the adverse pressure gradient case the skin friction coefficient, and correspondingly the friction velocity, is lower than the non-tilted case. At the same time, the velocity profile results less full. It is reasonable to assume that both the velocity U and the friction velocity manifest the same relative decreasing, therefore U^+ remains constant. This means that the difference in the law of the wall between the two cases is represented by the slope in the semi-logarithmic diagram; particularly, the slope decreases for the tilted plate respect to the zero-pressure gradient case, on the consequence the von Karman's constant decreases as well.

It has to be noted that this effect is more evident at high pressure gradient values [30].

VI. Results and Correlations

6.1 Introduction

In the present chapter many of the achieved results will be shown. The Chapter is developed into three main sections.

At first, several roughness parameters are shown for all plates, focusing the attention on the shape/density parameter that is estimated in the present work. Following, many boundary layer parameters are presented for all plates at the different test conditions analyzed. In this section is therefore visible the effect of roughness and the various boundary layer entities are also compared between all plates. Furthermore, laws of the wall are assessed for all cases, both smooth and rough ones.

All correlations achieved during the present research are shown in the third section.

6.2 Surface Roughness Parameters

As already stated, the experimental analysis of the surface texture allows to achieve many roughness parameters. All of them are carefully analyzed as to reproduce for each plate the surface texture, and to exploit the influence of a single parameter on the boundary layer flow features. The surface of the plates was manufactured in such a way that the effect of a roughness parameter alone could be cross-compared between the plates. Particularly, if the texture is mainly described through R_a and PF, which represent two different roughness scales, then it is always possible to compare two plates each other, by varying only one of the two parameters.

Values of both peak feed (PF) and mean roughness (R_a) are shown in figure 6.1, for all rough plates tested.

As previously stated, many roughness parameters are computed and compared between all plates, but not all of them are shown in this section, in order to focus the attention on one of the main results, i.e. the shape/density parameter currently achieved. The main purpose of the author is to exhibit the final results that have a direct application, while reducing the presentation of all those partial results that have been obtained when developing the present research, thus reducing the number of charts shown.

After all, an important consideration can be stated. All surfaces analyzed show a positive skewness value, which is typical of surface blade on duty. As a matter of fact, when a turbine operates small deposits increasingly accumulate over the surface and create a texture which is more high peaks based (i.e. positive skewness) than deep valleys based (i.e. negative skewness).
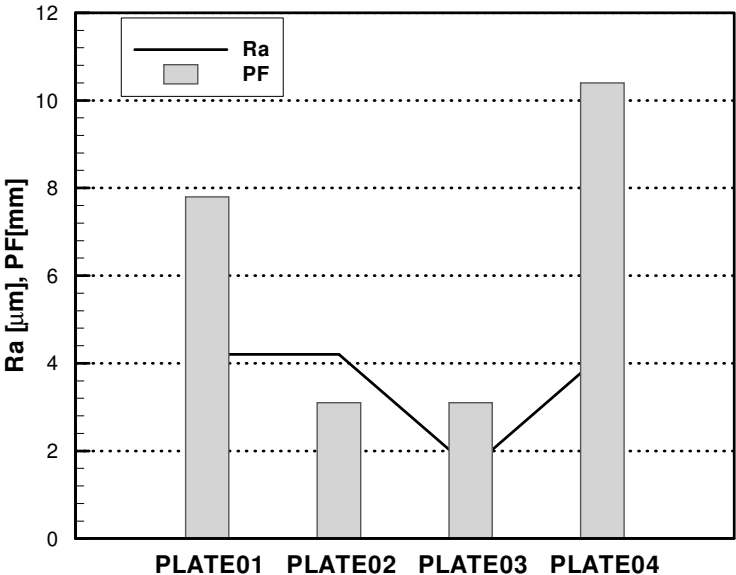

Figure 6.1 Required values of peak feed *PF* and mean roughness *Ra*.

6.2.1 Shape/Density Parameter

As described on Chapter V, the shape/density parameter for the tested rough plates is estimated after assuming a simplified roughness geometry as representative of the texture of the plates. This calculation is made using the available experimental data. Following the analytical expressions of the four surface areas that define the shape/density parameter are presented.

$$\Lambda_s = \frac{S}{S_f}\left(\frac{A_f}{A_s}\right)^{-1.6}$$

$$S = S_m \left(S_m\right)_q$$

$$S_f = \frac{\left(\dfrac{S_m}{2} R_{pm}\right)_q}{\cos \beta}$$

$$A_f = S_f$$

$$A_s = S_s = 2 \cdot \left(S_m\right)_q \left[\left(\frac{S_m}{2}\right)^2 + R_{pm}^2\right]^{\frac{1}{2}} \Big/ \cos \beta$$

The subscript q denotes roughness entities that are measured in a direction normal to the grooves main direction.

The equations written above are defined from few typical roughness parameters, and also from the *staggering* angle β. It is worth noting that the reference area S refers to a homologous smooth surface, therefore it is independent from the *staggering* angle.

It has to be underlined the importance of the relations found in the present research, since it appears that the shape/density parameter is a function of the following entities:

$$\Lambda_s \propto \left[\frac{S_m}{\left(R_{pm}\right)_q}\right]^{2.6} \cos \beta$$

The relation above refers to some observations made, which state as follows:

$$S_m \gg R_{pm}$$

$$\left(S_m\right)_q \gg \left(R_{pm}\right)_q$$

It is interesting to note that Λ_s is not influenced by the mean spacing estimated perpendicularly to groove direction, i.e. $(S_m)_q$. The latter is directly linked with the manufacturing parameter *PF*, therefore peak feed is not directly influencing the shape/density parameter, even if $(R_{pm})_q$ is related with the manufacturing process employed when grooving the surfaces.

From the proposed expression of the shape/density parameter a slight influence of the *staggering* angle is also visible. This effect is less evident on the arbitrary roughness height, which is obtained from Λ_s, as following shown in this chapter.

The shape/density parameter of all plates is shown in figure 6.2 for the case of the grooves aligned with the flow direction.
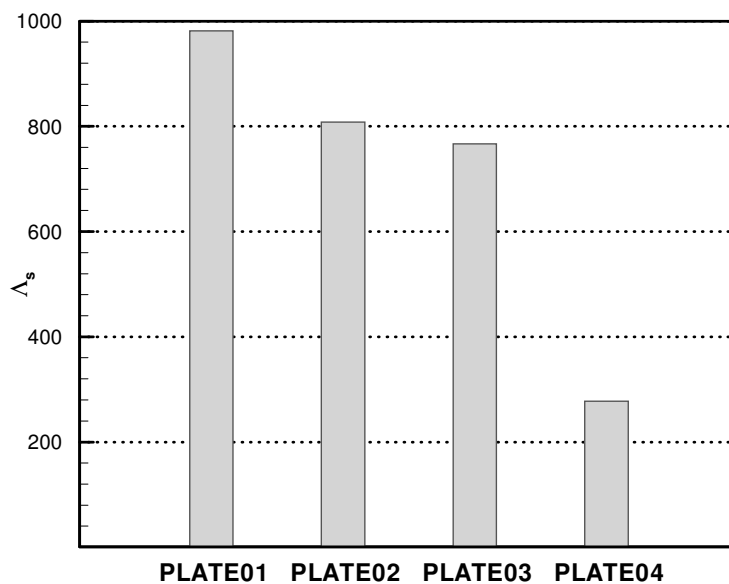
Figure 6.2 Shape/density parameter for all plates, $\beta = 0°$

6.3 Boundary Layer Features

A self-similar behavior of the velocity profile, at different Reynolds numbers, is observed in the central part of the plate, as visible in the non-dimensional diagram of figure 6.3, where all measuring points, for the axial position X_3, are fairly collapsing. It is also shown a perfect agreement with empirical values [56].

The self-similar behavior is not observed near leading edge and trailing edge, where positive and negative pressure gradient effects are respectively observed. Especially the first axial position is influenced by leading edge presence, which causes velocity to increase.

Figures 6.4-6 shows the influence of roughness on the velocity profile for all Reynolds numbers tested. Roughness influence is visible only at high Reynolds numbers, as visible in figure 6.6, where it is also noticeable the different behavior of plate 02.

In the following a series of issues from data analysis can be traced:

- Influence of roughness is noticed when comparing velocity profiles in different plates. In general, flow over rough surfaces is characterized by a steeper velocity profile than the corresponding one referred to smooth cases.
- Velocity profile for rough surfaces is less full than the corresponding one for smooth surfaces. In the former case boundary layer is thicker, consequently higher losses are observed.
- Roughness enhances transition, as can be found analyzing the velocity profile measured near the leading edge for the lowest Reynolds number tested.

It is worth to remind that the definition of hydraulically smooth plate, $k_s/\delta_v < 5$, was originally formulated for a plate having an homogeneous roughness caused by the deposition of

constant diameter sand grains on it. Therefore, this is a very special case that cannot be directly applied also to random-roughly plates. In general, a surface is considered hydraulically rough when the peaks of sandgrain roughness exceed the thickness of the viscous sublayer; in this way, the main flow can feel the asperities of the surface and be influenced by them. Moreover, it is proven that roughness influences the turbulent velocity fluctuations, being a source for turbulence production and increasing the Reynolds stress. Following this reasoning, it can be stated that if roughness peaks do not protrude over the viscous sublayer then roughness (at least the sandgrain type of it) cannot influence the main flow because the viscous effects are dominant. If this definition is applied to a general roughened surface, hence the most representative parameter to be compared with δ_v must represents the highest peaks, the ones that can emerge from the viscous sublayer and influence the turbulence inside the outer layer. For this purpose R_a cannot be the most representative parameter, while R_{tm} could be really appropriate. As already stated, real roughness can be very complex and not only the height of the peaks but also their distribution over the surface and their shape can be relevant. The shape/density parameter defined in this work can complete the description of the surface texture.

In order to fully understand the effects of surface roughness on the overall flow losses, it is worth considering integral boundary layer parameters, which give comprehensive information on the flow field inside the boundary layer.

Figure 6.14 shows the influence of Reynolds number on boundary layer displacement thickness for plate 04: as Reynolds number increases boundary layer becomes thinner, therefore losses are reduced.

Momentum thickness for a turbulent boundary layer is influenced by roughness, as shown in figure 6.17 for the highest Reynolds number tested, where all values are put in non-dimensional shape through the plate length c.

As already stated, roughness is not causing loss variation at the two lowest Reynolds numbers tested (figures 6.15-16).

Shape factor is shown in figure 6.18, in order to compare the experimental values of the smooth plate with the numerical results given by MISES code. Influence of roughness is not visible from the shape factor, since this parameter is the ratio between two integral parameters.

Skin friction coefficient for the analyzed cases is estimated using the procedure described on Chapter V, and it is plotted in figures 6.19-21.

Together with the experimental values of skin friction coefficients, it is also quoted the corresponding empirical curve. This is obtained for a zero-pressure gradient turbulent boundary layer on a smooth surface. Smooth plate results for all Reynolds number tested are in agreement with the empirical curve, except for the last two axial positions tested (X_4 and X_5). As previously explained, towards the trailing edge of the plate there is a negative pressure gradient that causes freestream velocity locally to increase.

Roughness influence is not evident at the lowest Reynolds number tested (see figure 6.19): viscous sublayer thickness found from data reduction is higher than the roughness height, therefore surface irregularities cannot strongly exhibit their disturbance on the flow.

At the first axial location, figure 6.19 shows for all plates lower values of the skin friction coefficient respect to the corresponding empirical ones. At the very low axial Reynolds number estimated in X_1, the flow is not turbulent but is still on transition. Moreover, as stated before, figure 6.19 shows how roughness enhances transition.

Figure 6.21 is also showing that skin friction coefficient for plate 01 at X_1 has not a reasonable value: the analysis of experimental data suggests that the achieved boundary layer parameter C_f is affected by a not-expected measurement error.

All boundary layer integral parameters analyzed confirm the roughness influence seen on the velocity profiles investigations.

Particularly, it is evident that Plate 02 is showing highest losses.

6.3.1 Law of the Wall

Starting from the experimental estimation of sandgrain roughness effects made in 1933 by Nikuradse [53], many studies were made in the aim of understanding the aerodynamic influence of surface roughness. The main goal was to achieve a universal law for the velocity profile near the wall, in analogy with the logarithmic one universally accepted for smooth surfaces, as discussed on Chapter II.

The universal log-law is not valid anymore in the outer layer. In this region, at the edge of the boundary layer, the velocity profile has to approach the freestream value, therefore there is a change in the velocity profile and a consequent detach from the linear trend (wake effect). In the analyzed data, the latter feature is taken into account through Coles' analytical function [54]. In this way, all measured entities fairly agree with the universal law of the wall, as shown in figures 6.29-31. Moreover, from these figures, mainly at the higher Reynolds numbers, it can be noticed that the main difference between smooth and rough cases is the value of the y-axis intercept (B constant).

6.3.2 Tilted Plates

The self-similar behavior of the velocity profile is not observed, due to the presence of the slight pressure gradient along the plate, and this is visible on the velocity profiles curves (figure 6.7).

Moreover, respect to the zero-pressure gradient case, it is possible to observe a different shape of the velocity profile and a thicker boundary layer (figure 6.8).

The integral boundary layer parameters show a comparable trend respect to the non-tilted case, while the influence of

roughness is less evident due to the thicker boundary layer (figures 6.22-25). Furthermore, roughness influence is more evident at increasing axial locations.

As made for the non-tilted case, the comparison between experimental and numerical results of the smooth plate is exemplified by the shape factor shown in figure 6.24. Also in this case, a good agreement is noted.

An important conclusion is that roughness influence is clearly predominant respect to pressure gradient influence.

The law of the wall for the different cases is shown in figures 6.32-34. Since there is a moderate pressure gradient, the von Karman constant used in the regression curve is the same as the one of the non-tilted case. Therefore, roughness effect is manifested only by the value of the constant *B*. As it was expected, the law of the wall for the rough cases is comparable with the analogous non-tilted plates.

The texture of the surface is clearly unchanged respect to the zero-pressure gradient case (what is changing is only a flow condition), since any geometrical feature is modified. This means that the shape/density parameter is the one shown on paragraph 6.2.1.

6.3.3 *Staggered* Plates

The presence of the *staggering* angle, at least for the values tested, does not alter the effect of roughness at increasing Reynolds number, as shown for plate 02 by the velocity profiles of figures 6.9-11.

The rating of roughness influence between all plates is also preserved respect to the non-*staggered* case, as visible when comparing the same *staggering* angle between two or more plates (figures 6.12-13).

The boundary layer integral parameters confirm what is stated regarding the velocity profiles (figures 6.26-28).

It is observed a beneficial effect of the inclined grooves respect to flow direction only for high *staggering* angles and this is in accordance with past observations (both experimental

and numerical) among riblets effect on boundary layer flow [11].

This circumstance occurs for only few of the tested cases, as for plate 04 at Re_3, where it is visible a slight decrease in the boundary layer losses respect to the non-*staggered* case. Skin friction coefficient and law of the wall for the latter case are shown in figures 6.26.

The *staggering* angle influence for the latter case is also captured by the arbitrary roughness height value (k), which is dependent on the shape/density parameter.

The effect of riblets is a very complex phenomenon, as already stated in the present work, it is linked to vortices and instabilities that generate inside the flow, and cannot be described only by a geometrical parameter like the shape/density one. Nevertheless, the latter one can give reliable information on the surface texture, being an important tool for predicting boundary layer losses.

As a conclusion, it can be stated that the *staggering* angle has almost no effect on the boundary layer flow, as soon as its value remains relatively low (40°÷45°), while for higher inclinations of the grooves there could be a decreasing in the boundary layer losses as a consequence of the effect of riblets.

Even the law of the wall for the *staggered* cases confirms that there is no influence of the inclination of the grooves (figure 6.35), except for high *staggering* angles, where a slight influence is observed (figure 6.36).

6.4 Correlations

In order to directly estimate roughness effect through the law of the wall, the non-dimensional velocity profiles referred to rough plates are compared with the universal log-law for smooth surfaces. The experimental data, represented in figures 6.29-36, are reduced according to the procedure introduced on Chapter V. For each plate a linear fitting is performed and the slope is set equal to the von Karman constant. The difference

in the intercept value between smooth and rough cases is representative of roughness effects. Next step is to correlate this flow behavior with the representative roughness parameters discussed before. Velocity defect of the rough case respect to the smooth one is correlated with an arbitrary roughness height k, which is based on the relation proposed by Grigson [43]. Roughness height is following linked with some real roughness parameters. In this way a correlation between shape/density parameter and the arbitrary roughness height k is obtained:

$$k = C_1 \cdot \Lambda_S^{C_2} \cdot R_{tm}$$

With the following values of the constants:

$$C_1 = 0.0041$$

$$C_1 = 0.68$$

R_{tm} is the Average Maximum Profile Peak-to-Depth Height. It is found that this relation is in good agreement with experimental data.

Values of k for the non-*staggered* case are plotted in figure 6.37.

From the relation regarding the arbitrary roughness height, it is evident the direct influence of peak heights, which are the real entities that influence the flow. Average roughness is not appearing, showing that R_a can only give an indication of roughness magnitude. The relation is also suggesting that higher mean spacing value, S_m, increases roughness: this could be explained by the influence of surface irregularities, e.g. riblets on vortex formation. Such irregularities can split relatively big stretched vortices near the surface in smaller ones, thus increasing the turbulence level and reducing the influence of real viscosity. The latter phenomenon is enhanced the spatially closer the irregularities are, which means the smaller the mean spacing is.

Furthermore, k is defined respect to the measured roughness parameter R_{tm} [10], which is also known as R_z (DIN) or R_t. This represents the peaks (specifically the average total roughness),

and it is historically used as to compare technical and sandgrain roughness, as stated by Nikuradse [53,54].

Finally, it is observed that the flow losses are proportional to PF/R_a ratio, but this two variables are not sufficient to fully illustrate roughness effects.

The relation proposed by Grigson is plotted in figures 6.38-40, using the experimental data achieved. Again, there is a good agreement with the experimental value, except for plate 01 at Re_3 ($\alpha = 0°$, $\beta = 0°$), for the reason explained before.

All charts cited before are following shown.
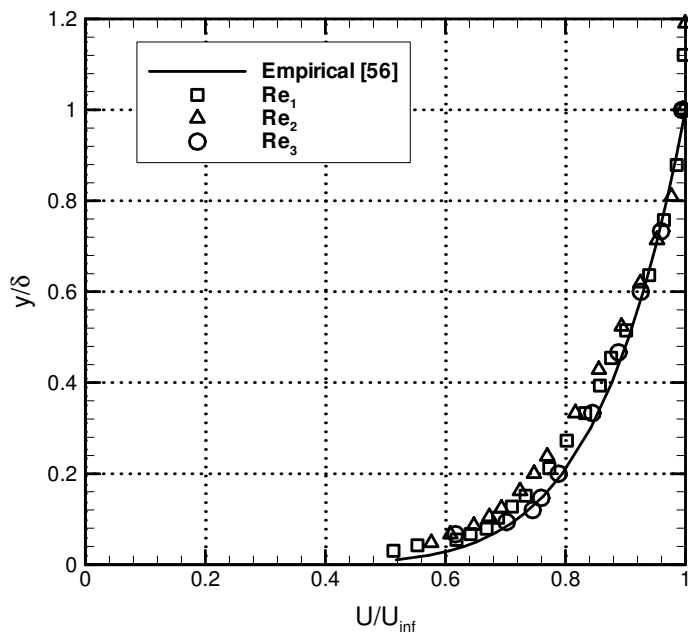
Figure 6.3 Non-dimensional velocity profiles at different Re, smooth plate, non-tilted case. Comparison with empirical law.
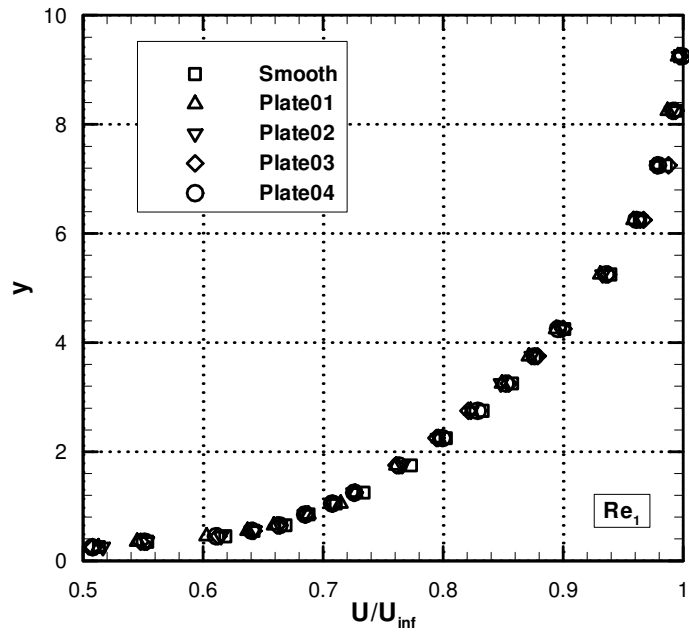
Figure 6.4 Velocity profiles for different plates (smooth and rough) at Re_1.
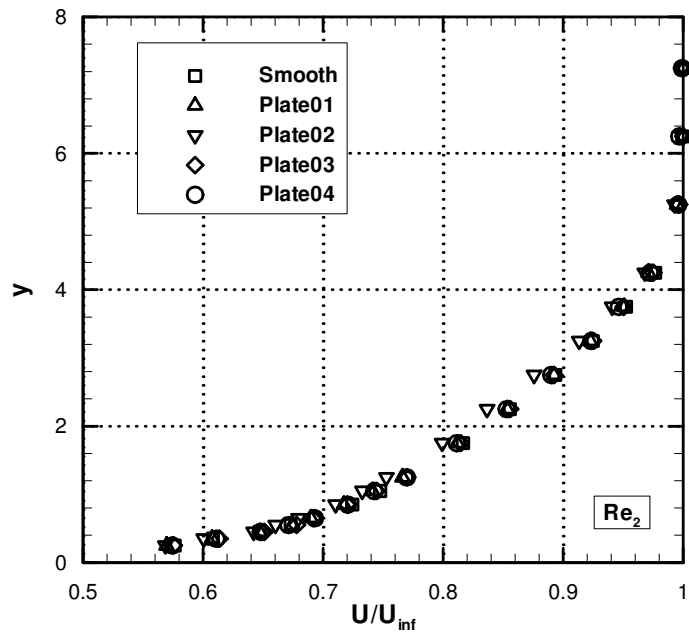
Figure 6.5 Velocity profiles for different plates (smooth and rough) at Re_2.
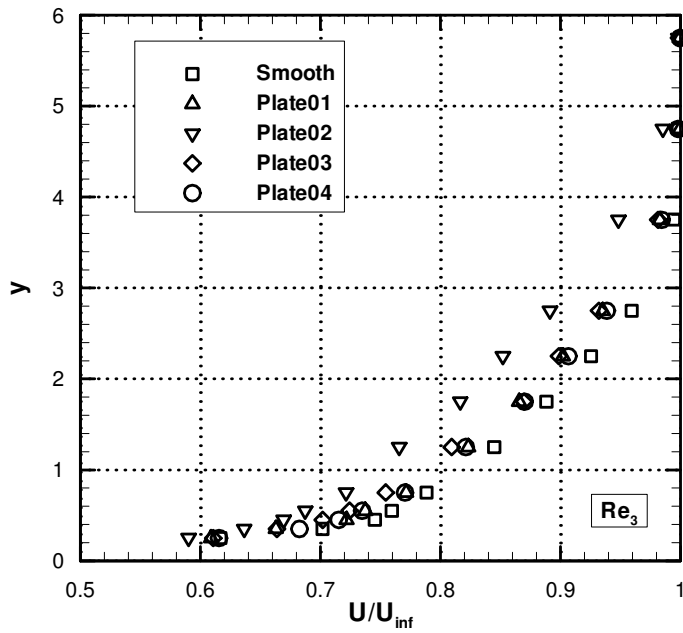
Figure 6.6 Velocity profiles for different plates (smooth and rough) at Re_3.
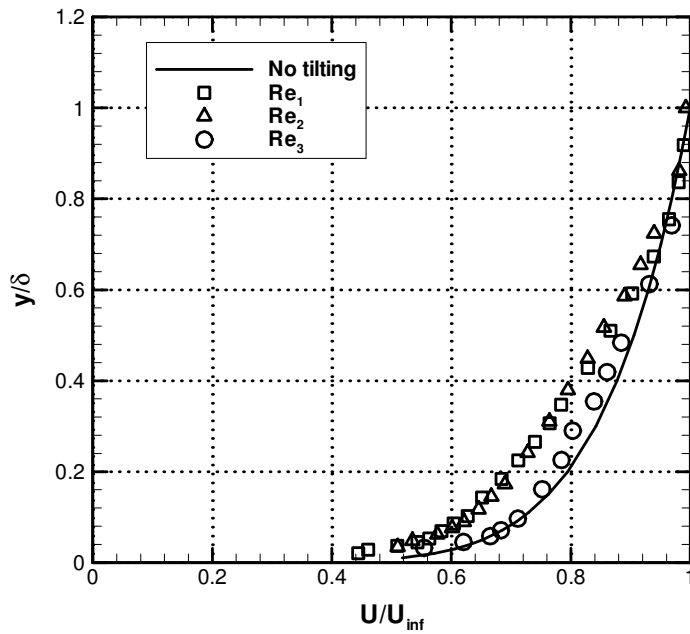
Figure 6.7 Non-dimensional velocity profiles at different Re, smooth plate, incidence angle 7°. Comparison with the non-tilted case.
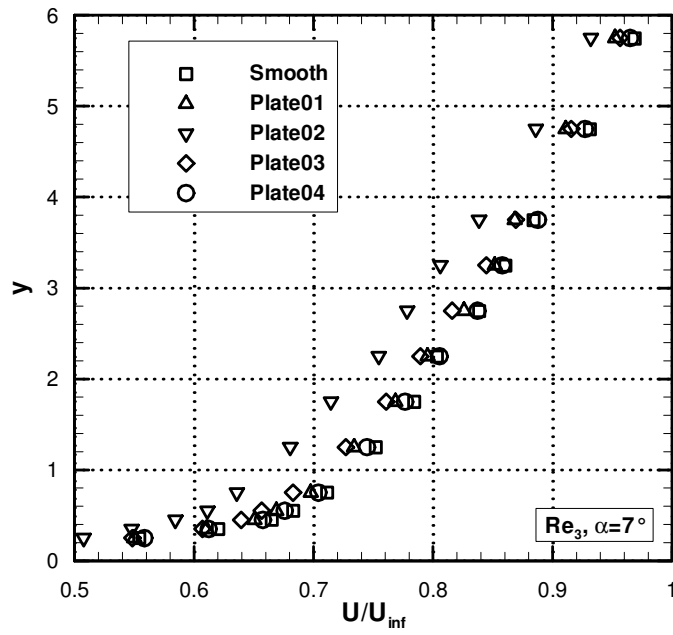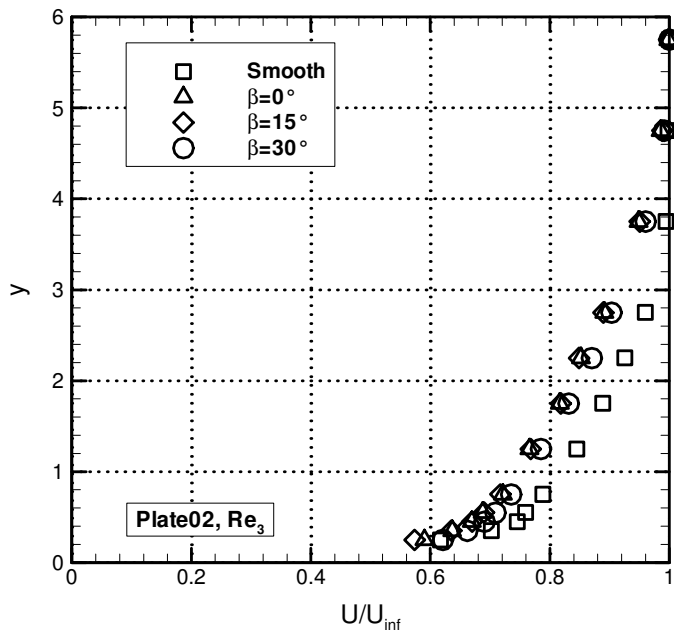
Figure 6.8 Velocity profiles for different plates (smooth and rough) at Re_3, incidence angle 7°.
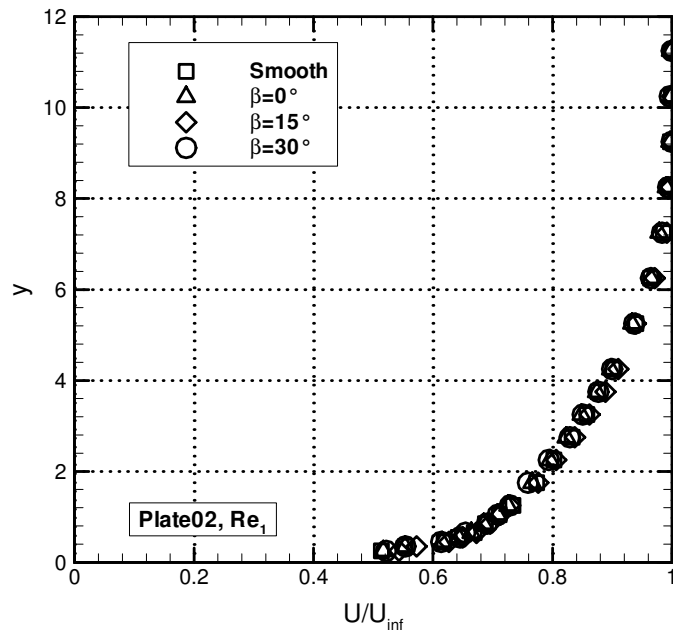
Figure 6.9 Velocity profiles for plate 02 at Re_1. Effect of the *staggering* angle.
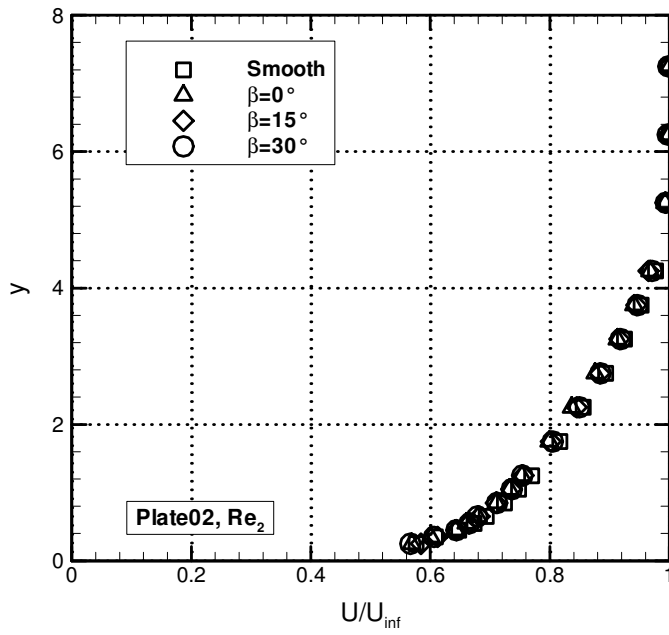
Figure 6.10 Velocity profiles for plate 02 at Re$_2$. Effect of the *staggering* angle.

Figure 6.11 Velocity profiles for plate 02 at Re$_3$. Effect of the *staggering* angle.

50
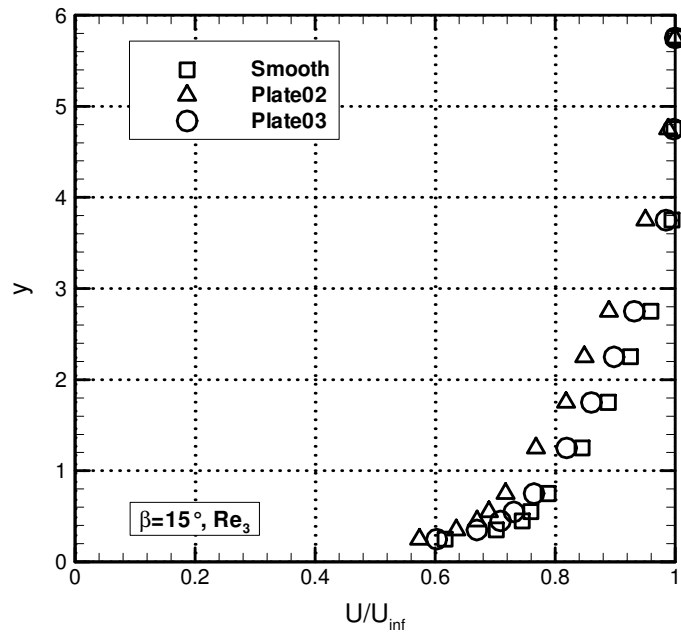
Figure 6.12 Velocity profiles for plate 02 and plate 03 at Re$_3$, $\beta = 15°$.
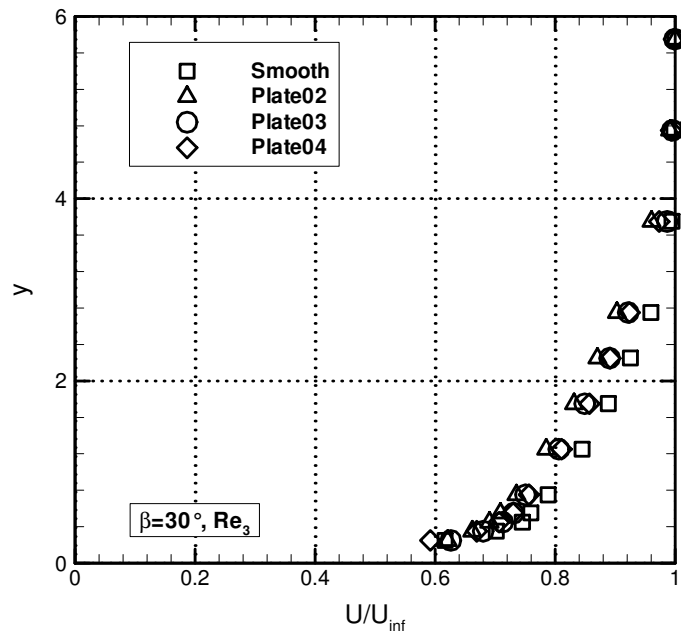
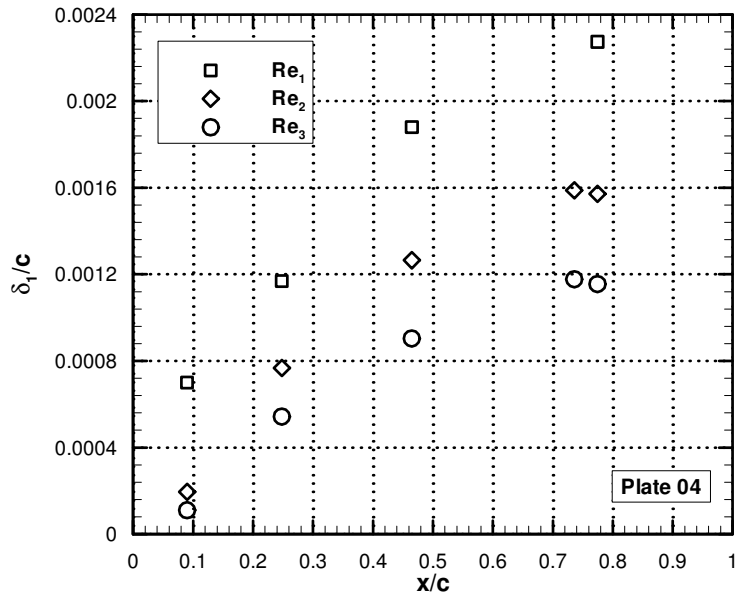**Figure 6.13** Velocity profiles for plate 02, plate 03 and plate 04 at Re$_3$, $\beta = 30°$.

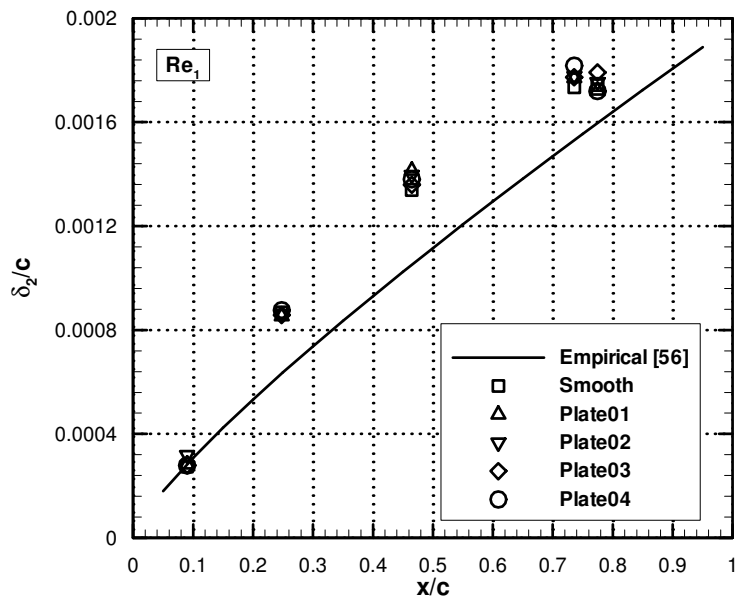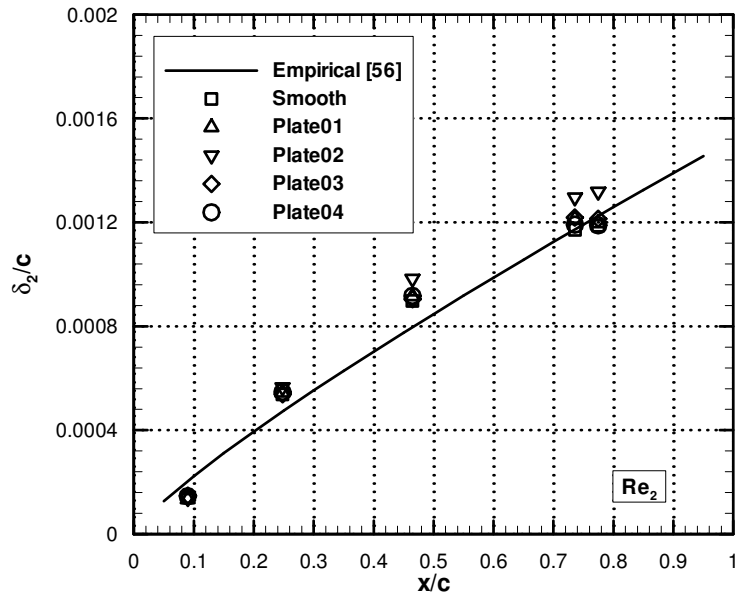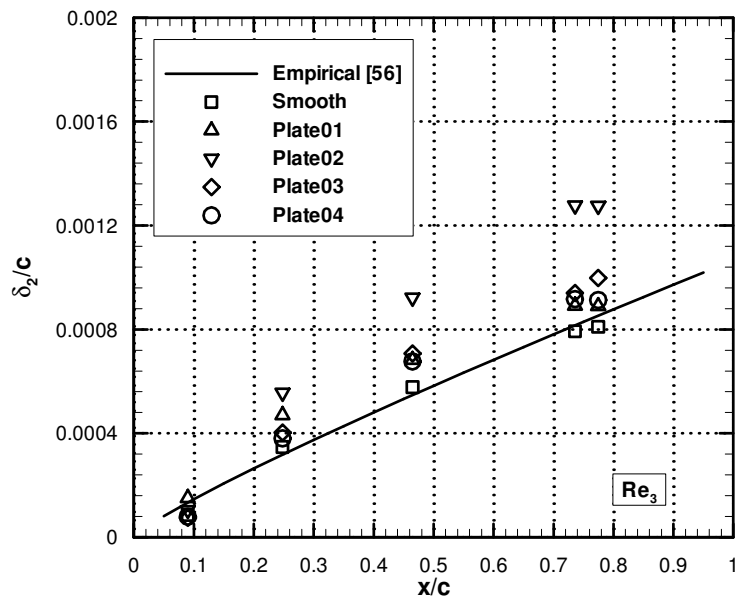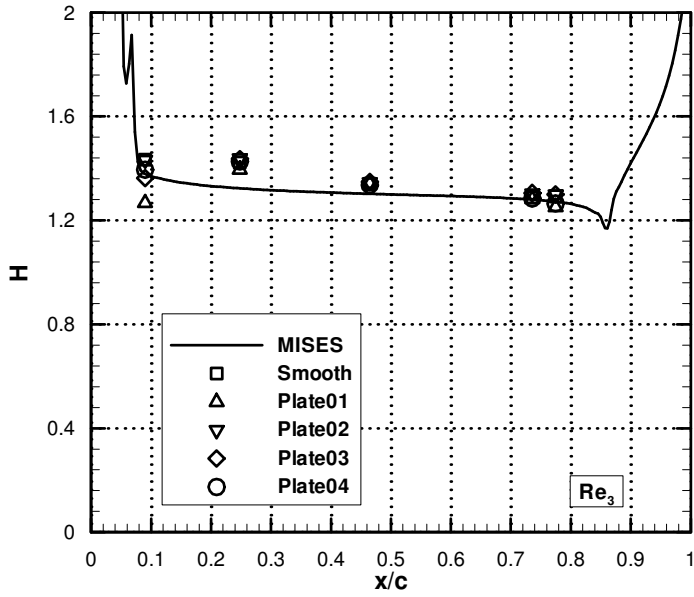**Figure 6.14** Displacement thickness: Reynolds number influence.

Figure 6.15 Momentum thickness for all plates at Re_1: comparison with empirical law and roughness influence.
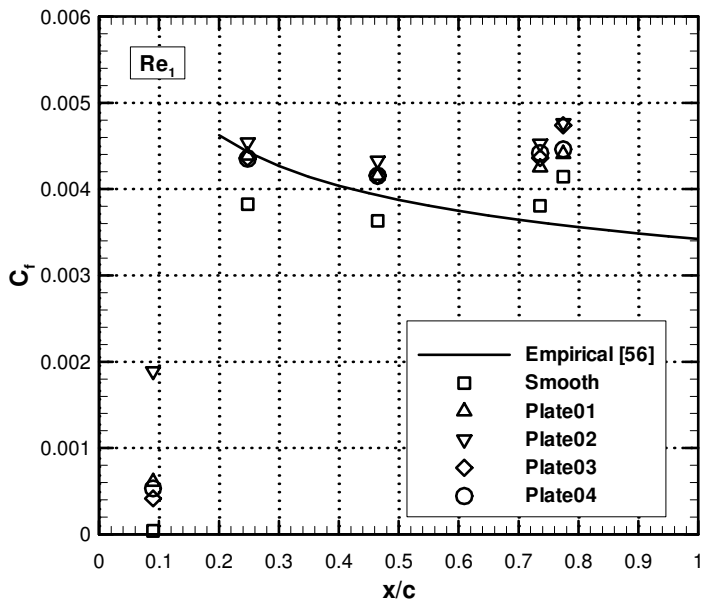
52

Figure 6.16 Momentum thickness for all plates at Re_2: comparison with empirical law and roughness influence.

Figure 6.17 Momentum thickness for all plates at Re_3: comparison with empirical law and roughness influence.

Figure 6.18 Shape factor for all plates at Re$_3$: comparison with numerical results (MISES).

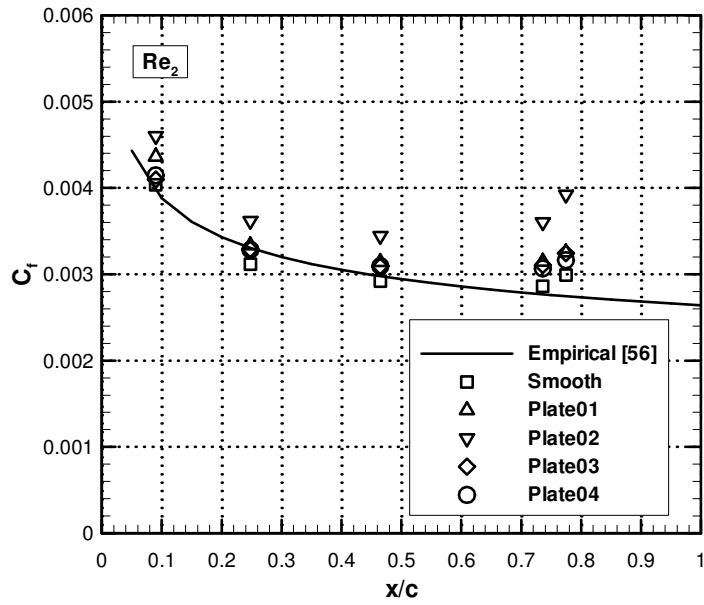**Figure 6.19** Skin friction coefficient for all plates, Re$_1$.

Figure 6.20 Skin friction coefficient for all plates, Re$_2$.

Figure 6.21 Skin friction coefficient for all plates, Re$_3$.

Figure 6.22 Displacement thickness: Reynolds number influence. Incidence angle 7°.
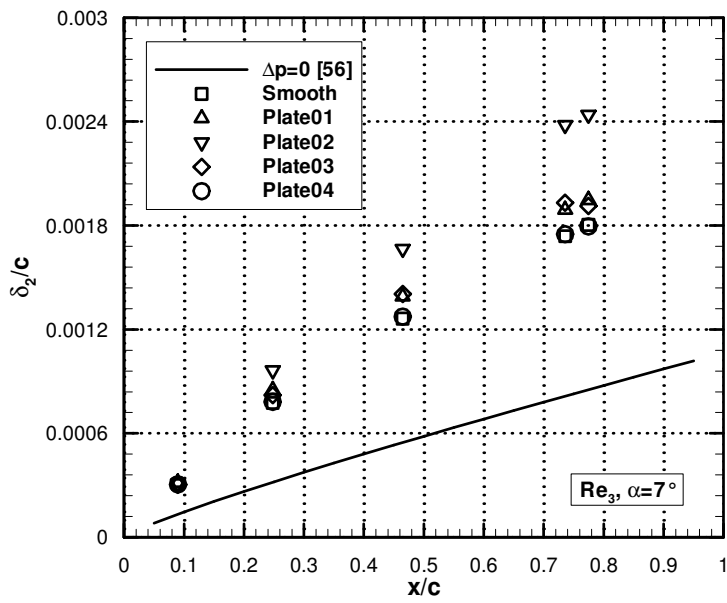
Figure 6.23 Momentum thickness for all plates at Re_3: comparison with empirical law and roughness influence. Incidence angle 7°.

56

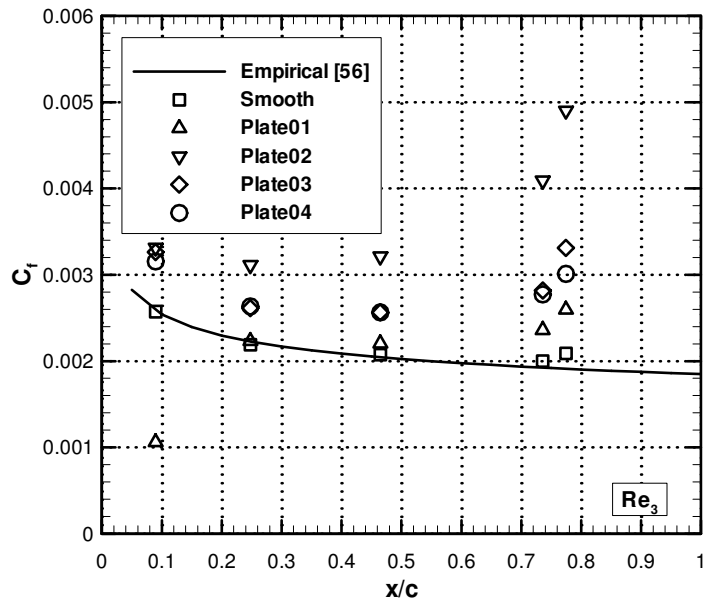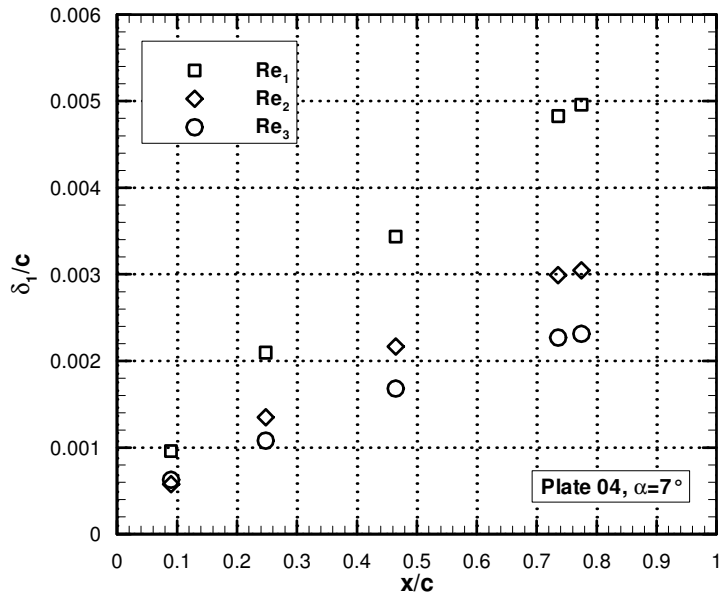**Figure 6.24** Shape factor for all plates at Re_3: comparison with numerical results (MISES). Incidence angle 7°.
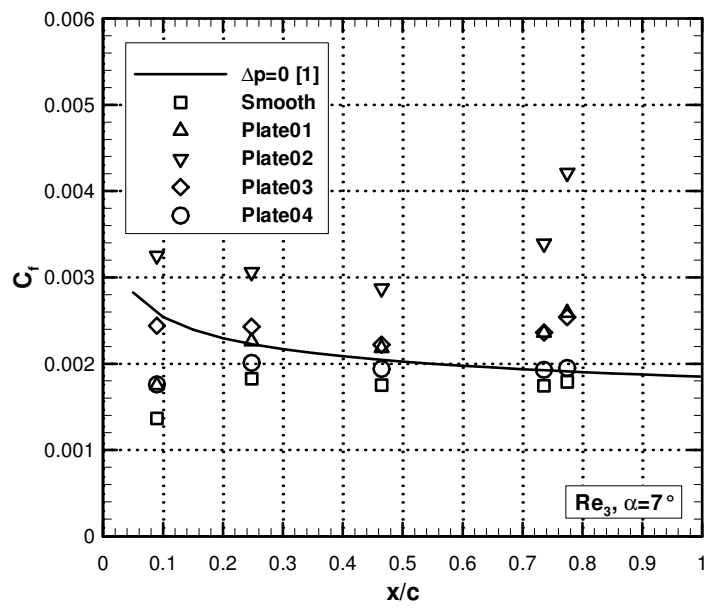
Figure 6.25 Skin friction coefficient for all plates, Re_3. Incidence angle 7°.
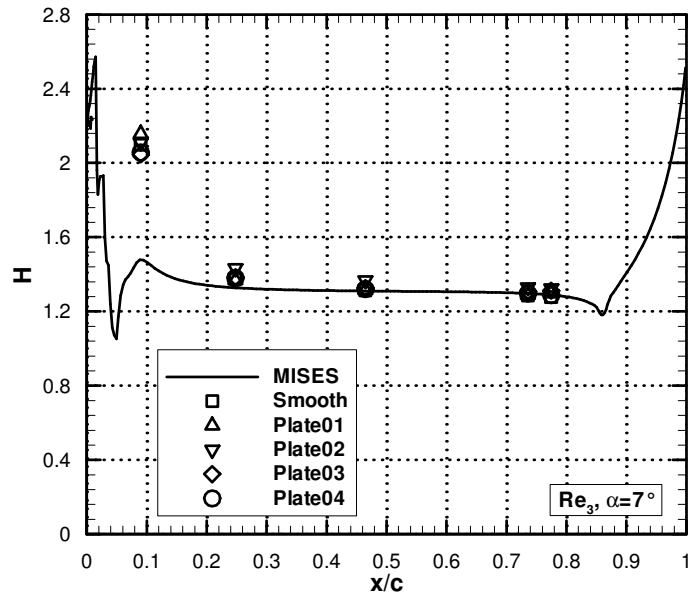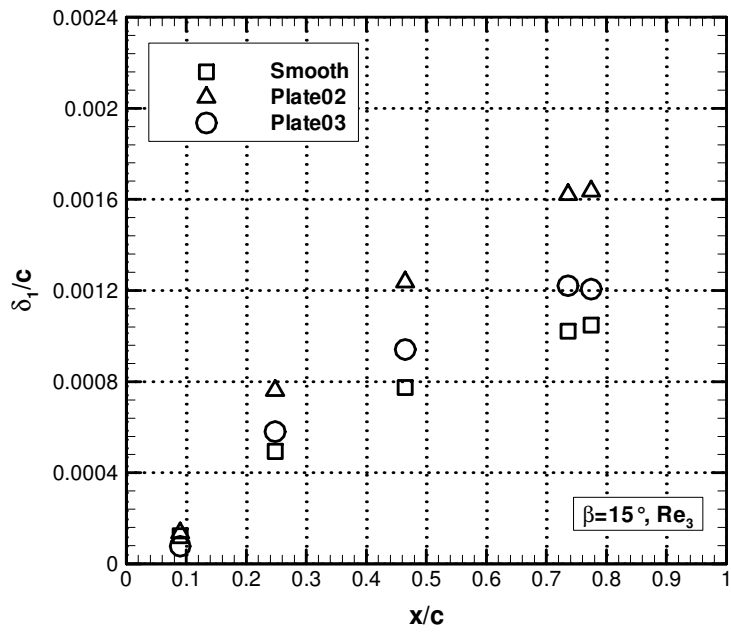
Figure 6.26 Displacement thickness for plate 02 and plate 03 at Re_3, $\beta = 15°$.
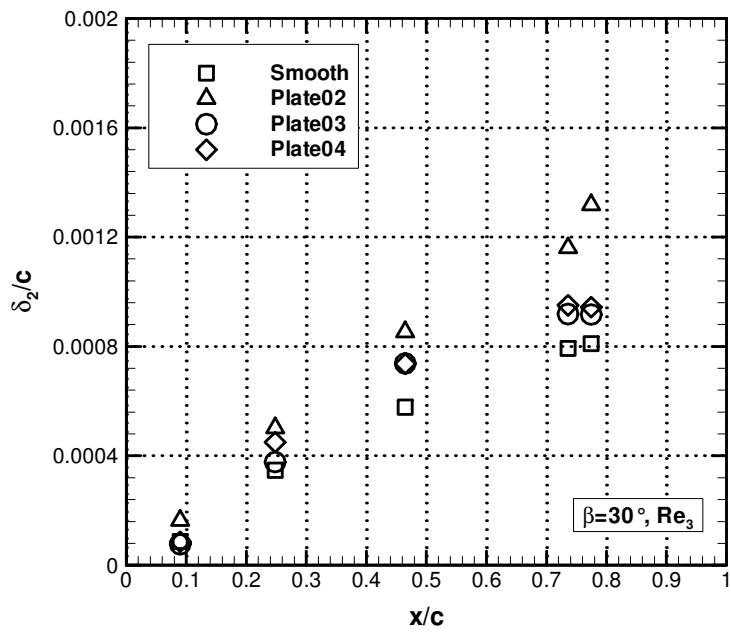
Figure 6.27 Momentum thickness for plate 02, plate 03 and plate 04 at Re_3, $\beta = 30°$.

58
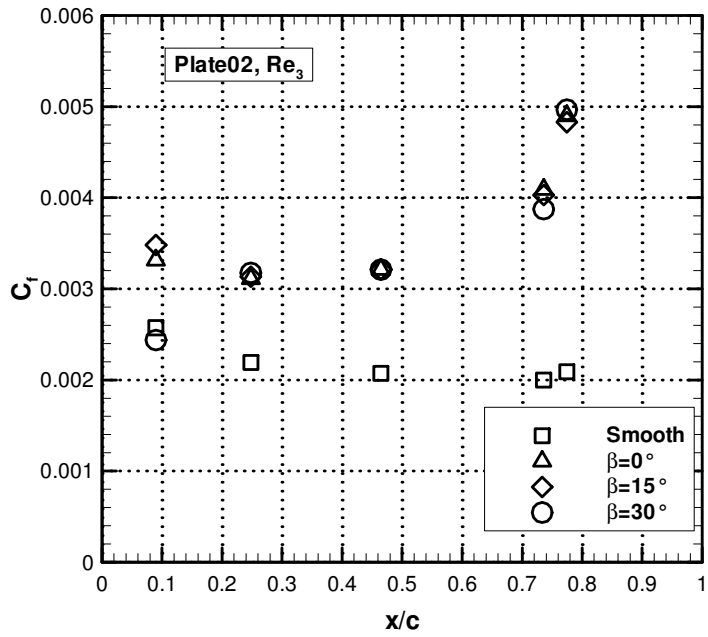
Figure 6.28 Skin friction coefficient for plate 02 at Re_3. Effect of the *staggering* angle.
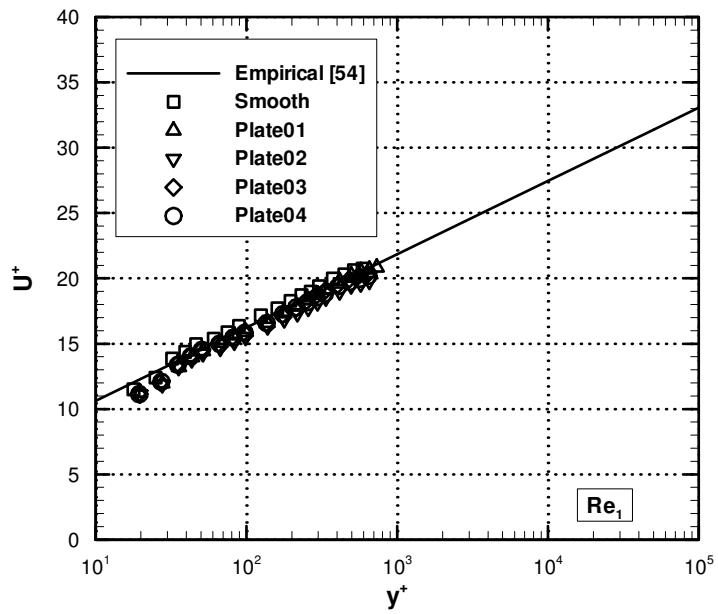
Figure 6.29 Law of the wall for all plates at Re_1.
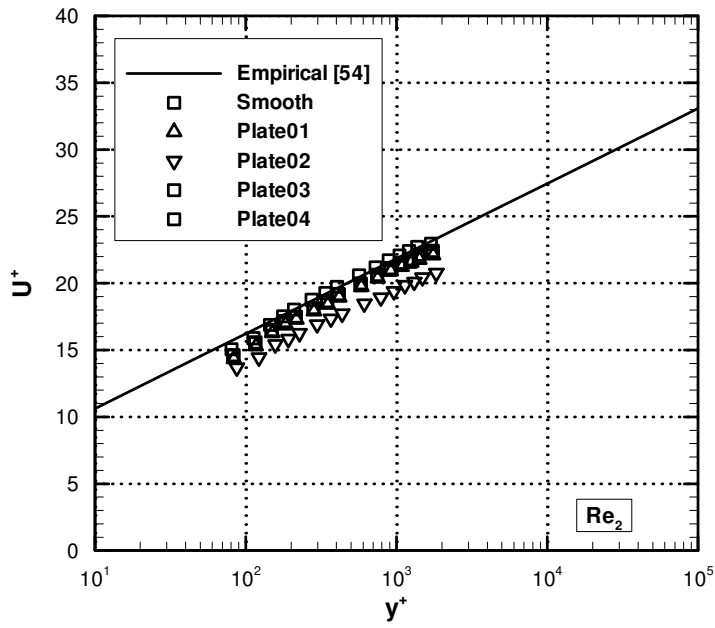
Figure 6.30 Law of the wall for all plates at Re$_2$.
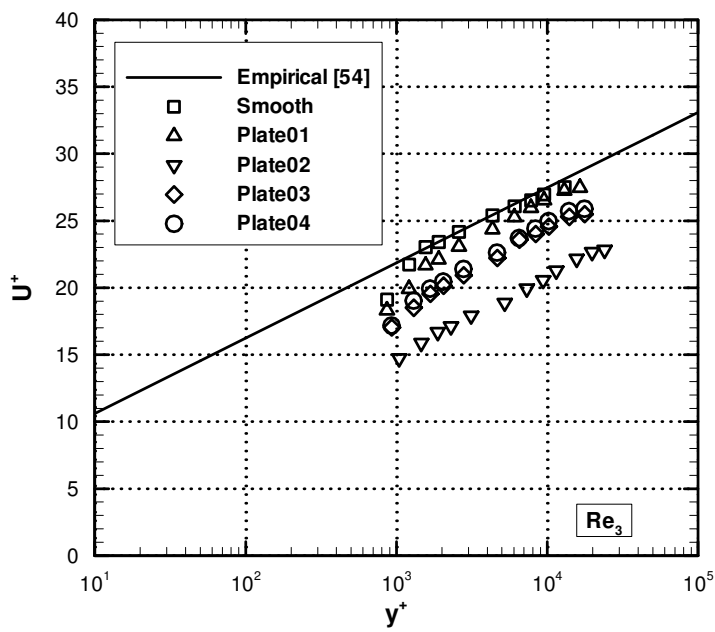
Figure 6.31 Law of the wall for all plates at Re$_3$.

60
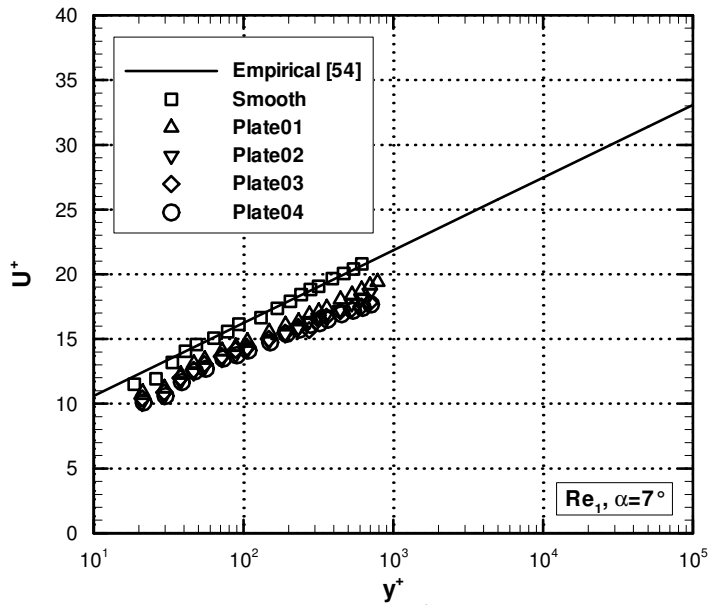
Figure 6.32 Law of the wall for all plates at Re_1. Incidence angle $7°$.
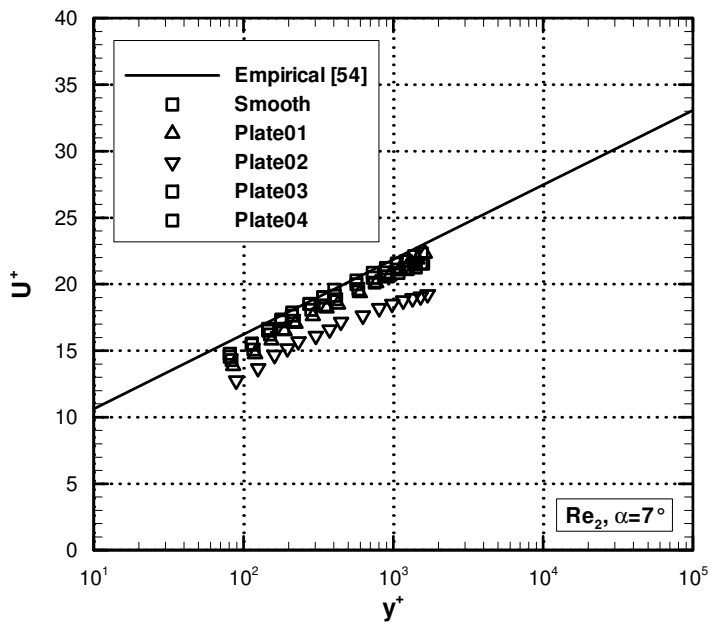
Figure 6.33 Law of the wall for all plates at Re_2. Incidence angle $7°$.
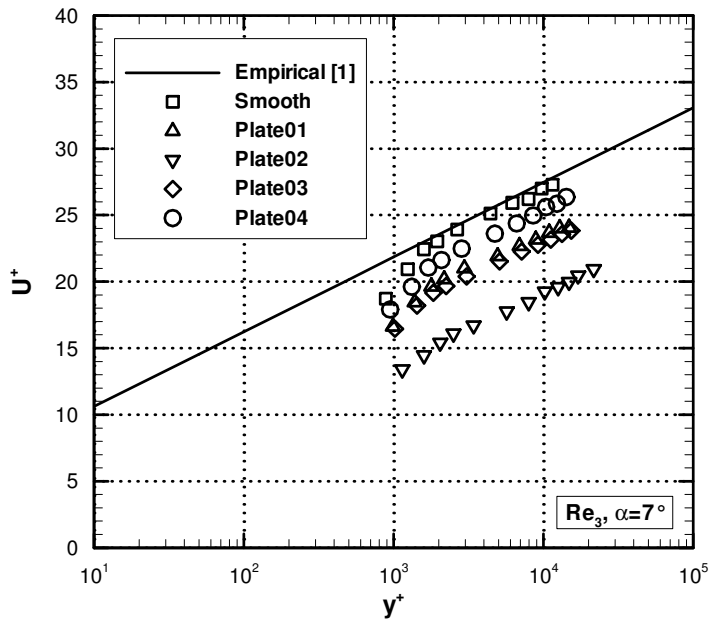
Figure 6.34 Law of the wall for all plates at Re$_3$. Incidence angle 7°.
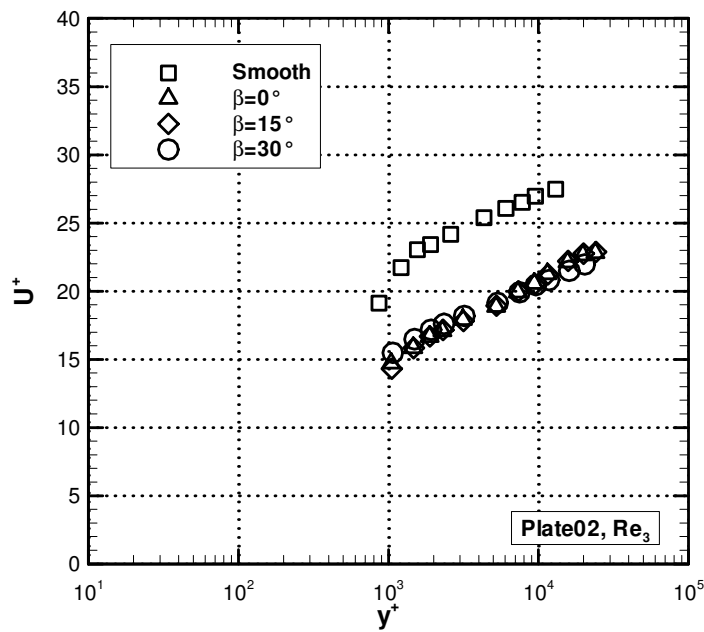
Figure 6.35 Law of the wall for plate 02 at Re$_3$. *Staggering* angle effect.
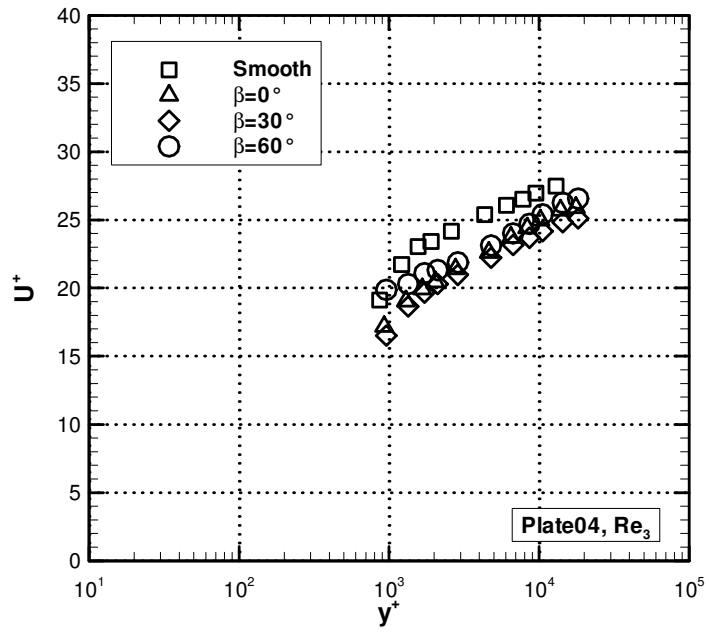
Figure 6.36 Law of the wall for plate 02 at Re$_3$. *Staggering* angle effect.
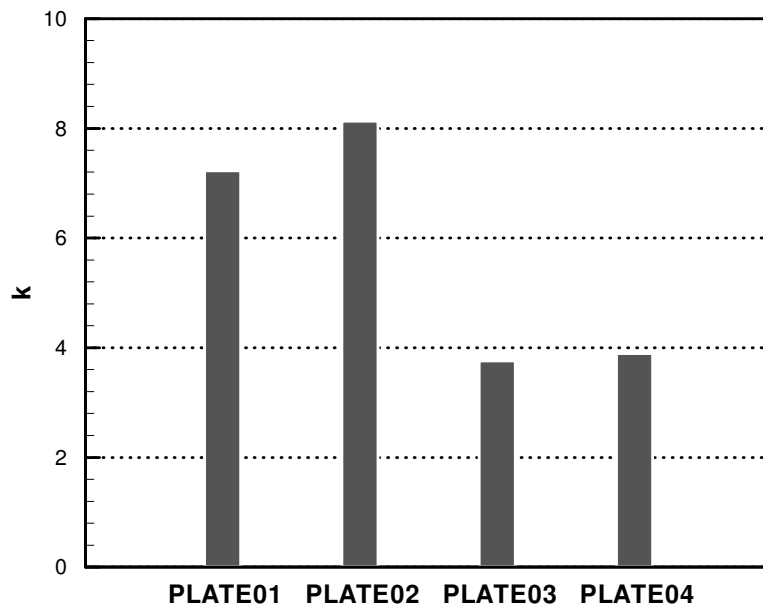
Figure 6.37 Arbitrary roughness height for all plates. Non-*staggered* case.
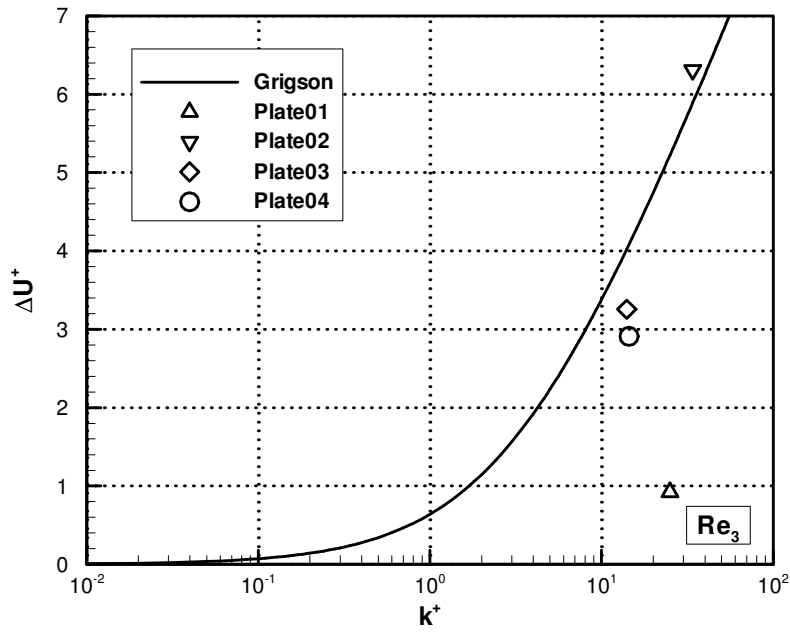
Figure 6.38 Correlation between velocity and roughness height for all plates at Re$_3$.
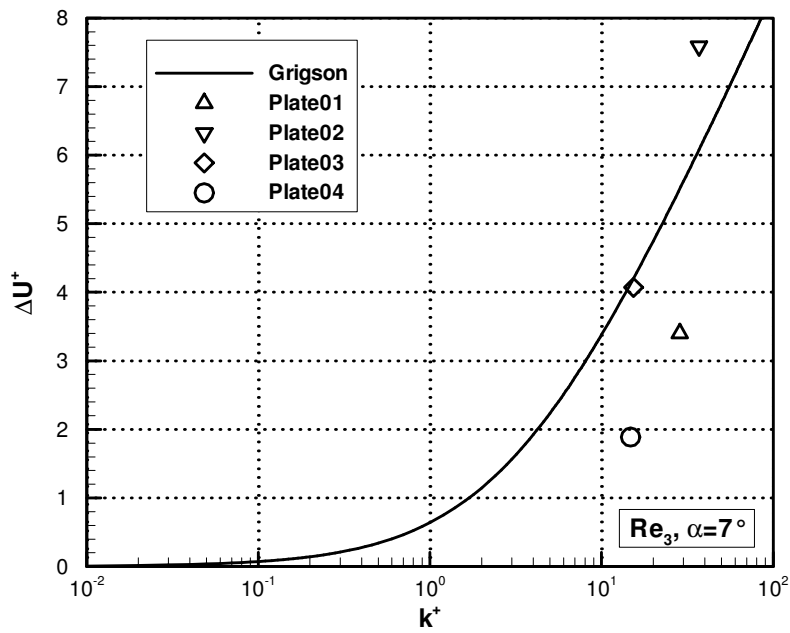
Figure 6.39 Correlation between velocity and roughness height for all plates at Re$_3$. Incidence angle 7°.
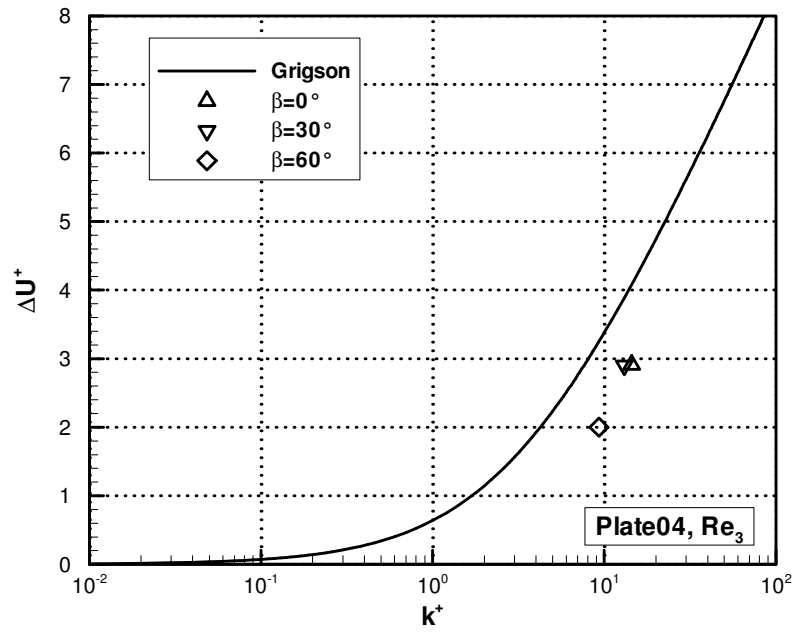
Figure 6.40 Correlation between velocity and roughness height for plate 04 at Re$_3$. *Staggering* angle influence.

VII. Concluding Remarks

7.1 Conclusions

This investigation was encouraged by the need to better understand the effects of surface roughness on the shear drag associated with turbine blading. Using facsimiles of real turbine blade surfaces, roughness statistics and flow characteristics over smooth and rough surfaces at three Reynolds number were analyzed. Main boundary layer features were estimated, showing roughness effects along five axial locations of the investigated plates. The texture of all rough plates is characterized by parallel grooves, and it was also investigated the influence on the boundary layer flow of the inclination of the grooves respect to flow direction. Moreover, the effect of freestream adverse pressure gradient was analyzed. Law of the wall for rough surfaces was achieved.

Many roughness parameters experimentally achieved over the surface of the plates were deeply investigated, in order to find a unique parameter, which is representative of surface texture, i.e. the shape/density parameter. In this way, it was possible to define an equivalent roughness height, which describes not only the amplitude of the asperities but also their shape and distribution over the surface.

Using the shape/density parameter a correlation of roughness characteristics with flow behavior inside the boundary layer was shown.

The various conclusions emerging from the experiments follow.

As discussed on Chapter III, the statistical descriptors associated with a given surface can provide great insight toward the surface's physical appearance. The average centerline roughness, R_a, commonly associated with equivalent sandgrain roughness, is often used to predict C_f, but, as

already noted [3, 5], appears inadequate in the specification of skin friction effects. While the majority of the statistical descriptors yielded insignificant relationships when compared to sandgrain roughness, the shape/density parameter appears to have a prevailing role in predicting boundary layer losses.

It was also found that increasing Reynolds number exacerbates the effects of roughness, as it was shown on Chapter VI by the boundary layer integral parameters.

Comparison between smooth and rough plates was correlated with the main roughness parameters, such as the equivalent roughness height k and the shape/density parameter Λ_s, and the result was graphically presented and compared with empirical law (Grigson).

Introduction of an adverse pressure gradient resulted in decreasing roughness effects.

When the grooves of the surface are inclined respect to flow direction, an appreciable influence on the boundary layer losses is perceived only at high *staggering* angle. This feature is also confirmed by the corresponding value of the equivalent roughness height. Therefore, the present work confirms that the presence of riblets over a surface causes loss reduction, as stated in previous works [11, 39].

It was confirmed, as previously stated [19], that the law of the wall, even if strictly not applicable, gives satisfactory results also on flows with mild streamwise pressure gradient and flows over ribletted surfaces.

7.1.1 Gas Turbine vs. Steam Turbine Blades

It is not the scope of the present research to underline the differences between gas and steam turbine blades, but the interest is on the boundary layer flow of the turbine blades and how surface roughness is affecting it.

There are several works [6, 14, 16, 42 and 44] on the effect of surface roughness on the boundary layer features of gas turbine blades, while very few researches were made on steam turbine [13]. The reason relies mainly on the experimental

difficulty to reproduce the testing condition typical of the high and intermediate pressure stages of steam turbines. Particularly, high Reynolds number and low roughness values are perceived. Besides, gas turbine blades need specific surface treatment in order to endure the heat loads and the corrosive environment of the exhaust gases. Roughness level is therefore very high (shown by the values of R_a and R_t) and it is even more intensified on service, as a consequence of the eroding process of the particles carried by the fluid. It has to be underlined the difference between the two types of fluids, the *clean* one flowing in the steam turbine blades has very few impurities compared with the fluid flowing in gas turbines.

Pitting and erosion, as said, are typical of gas turbine blades and are characterized by negative skewness values (surface texture has predominant deep valleys), therefore roughness influence is reduced, as it was exploited by the present work too.

Roughness is influencing the boundary layer flow over both steam ad gas turbine blades and it can be stated that it is possible to compare the two types of flow and to quantify the roughness influence, referring to non-dimensional entities like Reynolds number and appropriate roughness parameters.

7.2 Recommendations

The author tends to underline the importance of the experimental data in finding the correlations presented in the present work.

It should be further investigated the pressure gradient effect, mainly the one concerning negative incidence angle, through additional boundary layer measurements. This assessment would greatly benefit the understanding of turbine performance and efficiency.

The measurement campaign should also more deeply inspect the localized pressure gradient effects, which are visible near the leading edge and the trailing edge of the blade.

Moreover, it is suggested to continue analyzing the effect of riblets on boundary layer losses, especially at very high *staggering* angles.

It must be always kept in consideration the role played by the roughness-producing mechanism, e.g. deposits, erosion, pitting, and coating spallation, since they produce unique surface features that affect the flow in different ways.

Another aim is to give an indication for the limiting value of surface roughness below which the surface can be considered hydraulically smooth from a technical point of view. From a theoretical point of view, the latter circumstance occurs when k^+ is equal to zero (ΔU^+ as well), but as it was underlined also in the present work, the effect of roughness is remarkably visible only for high k^+ values.

For example, as it was shown in the present research, roughness is not influencing the flow at the Reynolds number Re_2, even if the viscous sublayer is thin respect to roughness peaks. Therefore, it would be useful to find the couple of values $(k^+, \Delta U^+)$ below which any roughness influence is perceived.

References

1. Ellering C.P., 2002, *The Combined Effect of Freestream turbulence, Pressure Gradients, and Surface Roughness on Turbine Aerodynamics*. Air Force Institute of Technology, Wright-Patterson AFB, Ohio.

2. Drab J.W. and Bons, J.P., 2002, *Turbine Blade Surface Roughness Effects on Shear Drag and Heat Transfer*, AIAA Paper No. 2002-0085

3. Acharya M., Bornstein J. and Escudier M.P., Spring-Summer 1986, *Turbulent Boundary Layers on Rough Surfaces*. Experiments in Fluids, **4**: 33-47.

4. Bennet J.M., Mattsson L., 1989*, Introduction to Surface Roughness and Scattering*. Washington DC: Optical Society of America.

5. Bogard D.G., Schmidt D.L., Tabbita M., April 1998*, Characterization and Laboratory Simulation of Turbine Airfoil Surface Roughness and Associated Heat Transfer*. ASME J. Turbomachinery, **120**: 337-342.

6. Bons J.P., Taylor R.P., McClain S.T., River R.B., April 1998, *The Many Faces of Turbine Surface Roughness*. ASME J. Turbomachinery, **123**: 739-747.

7. Kornilov V.I., Litvinenko Yu.A., Pavlov A.A., 2002, *Skin-Friction Measurements in An Incompressible Pressure-Gradient Turbulent Boundary Layer*.

8. Harbecke U., Riess W., Seume J., 2002, *The Effect of Milling Process Induced Coarse Surface Texture on Aerodynamic Turbine Profile Losses*. Proceedings of IGGT 2002.

9. Bergstrom D.J., Kotey N.A., Tachie M.F., 2002, *The Effects of Surface Roughness on the Mean Velocity Profile in a Turbulent Boundary Layer*. ASME J. Fluids Eng. **124**, pp. 664-670.

70

10. Van Rij J.A., Belnap B.J., Ligrani P.M., 2002, *Analysis and Experiments on Three-Dimensional , Irregular Surface Roughness*. ASME J. Fluids Eng. **124**, pp. 671-677.

11. Cousteix J., 1994, *Turbulence Management*. Computational Fluid Dynamics '94, pp. 159-168.

12. Riess W., Jetter C., *High-Quality Measurement Tecnique for Aerodynamic Characteristics of Turbine Blade Profiles*. Institute of Turbomachinery, University of Hanover.

13. Jonas O., Steltz W., Dooley B*., Steam Turbine Efficiency and Corrosion: Effects of Surface Finish, Deposits and Moisture*. EPRI.

14. Bons J.P., 2002, *St and Cf Augmentation for Real Turbine Roughness With Elevated Freestream Turbulence*. ASME J. Turbomachinery. **124**, pp. 632-644.

15. Cui J., Patel V.C., Lin C-L, 2003, *Prediction of Turbulent Flow Over Rough Surfaces Using a Force Field in Large Eddy Simulation*. ASME J. Fluids Eng. **125**, pp. 1-8.

16. Guo S.M., Jones T.V., Lock G.D., Dancer S.N., 1998, *Computational Prediction of Heat Transfer to Gas Turbine Nozzle Guide Vanes With Roughened Surfaces*. ASME J. Turbomachinery, **120**: 343-350.

17. Von Försching H., Melzer E., Schewe G., 1981, *Ein neuer Windkanal für gebäudeaerodynamische und aeroelastische Untersuchungen bei Reynoldszahlen bis 10^7*, konstruktiver ingenieurbau berichte, **35/36**: 127-133.

18. Wu S., Rajaratnam N., 2000, *A Simple Method for Measuring Shear Stress on Rough Boundaries*, Journal of Hydraulic Research, **38**: 399-400.

19. Baron A., Quadrio M., 1997, *On the Accuracy of Wall Similarity Methods in Determining Friction Velocity over Smooth and Ribletted Surfaces*. ASME J. Fluids Eng. **119**, pp. 1009-1011.

20. Acharya M., Escudier M.P., October 1984, *Turbulent Flow over Mesh Roughness*. Brown Boveri Rept KLR 84-179 C.

21. Acharya M., December 1985, *Pressure-gradient and Free-stream Turbulence Effects on Boundary-layer Transition*. Brown Boveri Rept KLR 85-127 C.

22. Harbecke U, 2001, *Aerodynamische Wirkung fertigungs-bedingter technischer Rauheiten und Geometriefehler an gefrästen Turbinenschaufeln*. Fortschritt-Berichte VDI.

23. Ghanipour A., (2004), Experimentelle Bestimmung der Grenzschichtparameter von spanabhebend gefertigten Oberflächen und numerische Modellierung., 225-2004 A 03A, 190 S

24. Wei N., 2000, *Significance of Loss Models in Aerothermodynamic Simulation for Axial Turbines*. KTH Doctoral Thesis, ISBN 91-7170-540-6

25. Brewer W.H., Park J.T, 2001, High Reynolds Number Boundary Layer Scaling on a Large Hydrofoil (HIFOIL). Naval Surface Warfare Center, Carderock Division, West Bethesda, MD.

26. Maydew R.C., Pappas C.C., 1952, *Experimental Evaluation of the Local and Average Skin Friction in the Laminar Boundary Layer on a Flat Plate at a Mach number of 2.4*. NACA, technical note 2740.

27. Crook A., 2002, *Skin Friction Estimation at High Reynolds Numbers and Reynolds-Number Effects for Transport Aircraft*. Center for Turbulence Research, Annual Research Briefs.

28. Gonzalez J.A., Melching C.S., Oberg K.A., 1996, *Analysis of Open-Channel Velocity Measurements Collected with an Acoustic Doppler Current Profiler*. 1st International Conference on New/Emerging Concepts for Rivers.

29. Nagib H., Christophoru C., Monkewitz P., 2004, *Impact of Pressure-Gradient Conditions on High Reynolds Number Turbulent Boundary Layers*. XXI ICTAM, Warsaw, Poland.

30. Fernholz H.H., Warnack D., 1998, *The Effect of a Favorable Pressure Gradient and of the Reynolds number on an*

incompressible axisymmetric turbulent boundary layer. *Part 1. The Turbulent Boundary Layer*. J. Fluid Mech. **359**, pp. 329-356.

31. Gustavsson J., 1998, *Experiments on Turbulent Flow Separation*. Master's Thesis, Royal Institute of Technology, Sweden.

32. Zhang Q., Lee S.W., Ligrani P.M., 2004, *Effects of Surface Roughness and Turbulence Intensity on the Aerodynamic Losses Produced by the Suction Surface of a Simulated Turbine Airfoil*. ASME J. Fluid Eng. **126**, pp.257-265.

33. A. Cheskidov, 2002, *Turbulent Boundary Layer Equations*. C.R. Acad. Paris, Ser. I 334 (2002) 423-427.

34. Du Z., Selig M.S., 1998, *The Effect of Rotation on the Boundary Layer of a Wind Turbine Blade*. Windpower '98 Conference.

35. Österlund J. M., 1999, *Experimental Studies of Zero Pressure-Gradient Turbulent Boundary-Layer Flow*. Doctoral Thesis, Royal Institute of Technology, Sweden.

36. Kang Y.S., Yoo J.C., Kang S.H., 2004, *Numerical Study of Roughness Effects on a Turbine Stage Performance*. ASME Turbo Expo 2003, GT2004-53750.

37. Craft T.J., Gant S.E., Gerasimov A.V., Iacovides H., Launder B.E., 2004, *Wall-Function Approaches for Turbulent Flow CFD*, 17th National and 6th ISHMT-ASME Heat and Mass Transfer Conference, Tamil Nadu, India.

38. Ham F.E., Lien F.S., Wu X., Wang M., Durbin P., 2000, *LES and Unsteady RANS of Boundary Layer Transition Induced by Periodically Passing Waves*. Center of Turbulent Research, Proceedings of the Summer Program 2000.

39. Ninnemann T., Ng W.F., July 2004, *Loss Reduction Using Riblets on a Supersonic Through-Flow Fsn Blade Cascade*. ASME **126**, pp.642-649.

40. Drela M., Giles M.B., October 1987, *Viscous-Inviscid Analysis of Transonic and Low Reynolds Number Airfoils*. AIAA Journal **25**, pp.1347-1355.

41. de Saint Victor X., Houdeville R., Aipoix B., March 2005*, Extenson of t he Spalart-Allmaras Model to Account for Wall Roughness. Application to Flow Over the T106 Blade*. 6th ETC, Lille, France.

42. Hummel F., Lötzerich M., Cardamone P., Fottner L., June 2004, *Surface Roughness Effects on Turbine Blade Aerodynamics*. ASME Turbo Expo, Vienna, Austria.

43. Schultz M.P., November 2004, *Frictional Resistance of Antifouling Coating Systems*. ASME J. Fluids Eng. **126**, pp. 1039-1047.

44. McClain S.T., Hodge B.K., Bons J.P., April 2004, *Predicting Skin Friction and Heat Transfer for Turbulent Flow Over Real Gas Turbine Surface Roughness Using the Discrete Element Method*. ASME J. Turbomachinery **126**, pp. 259-267.

45. Krogstad P. Å, Antonia R. A., February 1999, Surface Roughness Effects in Turbulent Boundary Layers. Experiments in Fluids, **27**: 450-460.

46. Lushchik V.G., Pavel'ev A.A., Yakubenko A.E., June 2003. *Transition to Turbulence in the Boundary Layer on a Plate in the Presence of a Negative Free-Stream Pressure Gradient*. Fluid Dynamics, **39**, pp. 250-259.

47. Balachandar R., Patel V.C., October 2002. *Rough Wall Boundary Layer on Plates in Open Channels*. J. Hydraulic Eng., **128**, pp. 947-951.

48. Antonia R.A., Luxton R.E., March 1971. *The response of a Turbulent Boundary Layer to an Upstanding Step Change in Surface Roughness*. J. Basic Eng., pp. 22-34.

49. Abuaf N., Bunker R.S., Lee C.P., July 1998. *Effects of Surface Roughness on Heat Transfer and Aerodynamic*

Performance of Turbine Airfoils. ASME J. Turbomachinery, **120**: 522-529.

50. Leipold R., Boese M., Fottner L., July 2000. *The Influence of Technical Surface Roughness Caused by Precision Forging on the Flow Around a Highly Loaded Compressor Cascade*. ASME J. Turbomachinery, **122**: 416-425.

51. Bergstrom D.J., Akinlade O.G., Tachie M.F., November 2005. *Skin Friction Correlation for Smooth and Rough Wall Turbulent Boundary Layers*. ASME J. Fluids Eng. **127**, pp. 1146-1153.

52. Bushmann M.H., Gad-el-Hak M., April 2003. *Debate Concerning the Mean-Velocity Profile of a Turbulent Boundary Layer*. AIAA J., **41**, No 4, pp. 565-572.

53. Nikuradse J., *Laws of flow in rough pipes*. VDI Forschungsheft No. 361 (1933): translated as British ARC paper 986 (1933), NACA TM 1292 (1950).

54. Schlichting H., 1979, *Boundary-Layer Theory.* McGraw–Hill, New York.

55. Cebeci, T. and Smith A.M.O., 1974, *Analysis of Turbulent Boundary Layers*. New York: Academic Press.

56. White F.M., 1974, *Viscous Fluid Flow*, McGraw-Hill, New York.

57. Sigal A., Danberg J.E., 1990, *The New Correlation of Roughness Density Effect on the Turbulent Boundary Layer*. AIAA J. **28**: 554-556.

58. Melis G., Cambuli F., Mandas N., 2006, *Skin Friction Correlation for real roughened Surfaces*. Proceedings of the 61th ATI Conference.

Appendix A – Surface Texture Parameters

The purpose of a parameter is to generate a number that can characterise a certain aspect of the surface, removing the need for subjective assessment. However it is impossible to completely characterise a surface with a single parameter. Therefore a combination of parameters is normally used.

Parameters can be separated into three basic types:

a) Amplitude parameters - these are measures of the vertical characteristics of the surface deviations.

b) Spacing parameters - these are measures of the horizontal characteristics of the surface deviations

c) Hybrid parameters - these are a combination of both the vertical and horizontal characteristics of the surface deviations.

A.1 Amplitude Parameters

The average roughness is the area between the roughness profile and its mean line, or the integral of the absolute value of the roughness profile height over the evaluation length L_m:

$$R_a = \frac{1}{L_m} \int_0^{L_m} |y(x)| dx$$

y is the vertical distance from the mean line.

Graphically, the average roughness is the area between the roughness profile and its center line divided by the evaluation length (normally five sample lengths with each sample length equal to one cutoff.

The root-mean-square (rms) average roughness of a surface is calculated from another integral of the roughness profile:

$$R_q = \sqrt{\frac{1}{L_m} \int_0^{L_m} (y(x))^2 dx}$$

For a pure sine wave of any wavelength and amplitude R_q is proportional to R_a; it's about 1.11 times larger.

R_q has now been almost completely superseded by R_a In metal machining specifications. R_q still has value in optical applications where it is more directly related to the optical quality of a surface.

The peak roughness R_p is the height of the highest peak in the roughness profile over the evaluation length.

$$R_p = \left|\max[y(x)]\right|, \quad 0 < x < L_m$$

R_v is the depth of the deepest valley in the roughness profile over the evaluation length.

$$R_v = \left|\min[y(x)]\right|, \quad 0 < x < L_m$$

The total roughness, R_t, is the sum of these two, or the vertical distance from the deepest valley to the highest peak.

$$R_t = R_p + R_v$$

Define the maximum height for the i-th sample length as R_{pi} and the average maximum profile peak height results:

$$R_{pm} = \frac{1}{M}\sum_{i=1}^{M} R_{pi}$$

Define the maximum depth for the i-th sample length as R_{vi}:

$$R_{vm} = \frac{1}{M}\sum_{i=1}^{M} R_{vi}$$

Sum of the last two parameters:

$$R_{tm} = \frac{1}{M}\sum_{i=1}^{M} R_{ti} = R_{pm} + R_{vm}$$

where R_{vi} is the depth of the deepest valley in the i-th sample length and R_{ti} is the sum of R_{vi} and R_{pi}:

$$R_{pi} = \left|\max[y(x)]\right|, \quad il < x < (i+1)l$$

$$R_{vi} = \left|\min[y(x)]\right|, \quad il < x < (i+1)l$$

$$R_{ti} = R_{pi} + R_{vi}$$

R_z(DIN), i.e. R_z according to the German DIN standard, is just another name for R_{tm} in the American nomenclature (over five cutoffs):

$$R_z[\text{DIN}] = R_{tm}$$

R_z(ISO) is the sum of the height of the highest peak plus the lowest valley depth within a sampling length.

$$R_{sk} = \frac{1}{L_m R_q^3} \int_0^{L_m} (y(x))^3 dx$$

R_{sk} is the skewness and indicates whether the surface consists of mainly peaks, valleys or an equal combination of both. It is the measure of the symmetry of the profile about the mean line. A surface with predominant peaks will be considered as 'positive skew' and a surface with predominant valleys will be considered as 'negative skew'. Negative skew, for example, is desirable where oil retention is required. Positive skew may be desirable where adhesion is required.

$$R_{ku} = \frac{1}{L_m R_q^4} \int_0^{L_m} (y(x))^4 dx$$

R_{ku} is called kurtosis and is a measure of the sharpness of the surface profile.

While R_{sk} is the third moment, R_{ku} is the fourth moment of the amplitude distribuitoin function ADF (probability function).

A.2 Hybrid Parameters

The following is the average of the absolute value of the slope of the roughness profile over the evaluation length:

$$\Delta_a = \frac{1}{L_m} \int_0^{L_m} \left| \frac{dy(x)}{dx} \right| dx$$

A.3 Spacing Parameters

S_m is the mean spacing between peaks, with a peak defined relative to the mean line. A peak must cross above the mean line and then back below it.

If the width of each peak is denoted as S_i, then the mean spacing is the average width of a peak over the evaluation length:

$$S_m = \frac{1}{N} \sum_{i=1}^{N} S_i$$

The average wavelength of the surface is defined as follows:

$$\lambda_a = 2\pi \frac{R_a}{\Delta_a}$$

This parameter is analogous to S_m in that it measures the mean distance between features, but it is a mean that is weighted by the amplitude of the individual wavelengths, whereas S_m will find the predominant wavelength.